Structure-Based Design of Inhibitors of Purine Nucleoside Phosphorylase. 1. 9-(Arylmethyl) Derivatives of 9-Deazaguanine

John A. Montgomery,*,†,‡ Shri Niwas,‡ Jerry D. Rose,‡ John A. Secrist III,‡ Y. Sudhakar Babu,† Charles E. Bugg,§ Mark D. Erion,∥,⊥ Wayne C. Guida,∥ and Steven E. Ealick§,⊕

BioCryst Pharmaceuticals, Inc., 2190 Parkway Lake Drive, Birmingham, Alabama 35244, Southern Research Institute, P.O. Box 55305, Birmingham, Alabama 35255-5305, Center for Macromolecular Crystallography, University of Alabama at Birmingham, University Station, Birmingham, Alabama 35294-2010, and CIBA-GEIGY Corporation, 556 Morris Avenue, Summit, New Jersey 07901

Purine nucleoside phosphorylase (PNP, EC 2.4.2.1) is a salvage enzyme important to the T-cell-mediated part of the immune system and as such is an important therapeutic target. This paper describes the design, synthesis, and enzymatic evaluation of potent, competitive inhibitors of PNP. Potential inhibitors were designed using the three-dimensional structure of the enzyme in an iterative process that involved interactive computer graphics to model the native enzyme and complexes of it with the inhibitors, Monte Carlo-based conformational searching, and energy minimization. Studies of the enzyme/inhibitor complexes were used to determine priorities of the synthetic efforts. The resulting compounds were then evaluated by determination of their IC_{50} values and by X-ray diffraction analysis using difference Fourier maps. In this manner, we have developed a series of 9-(arylmethyl)-9-deazapurines (2-amino-7-(arylmethyl)-4H-pyrrolo[3,2-d]-pyrimidin-4-ones) that are potent, membrane-permeable inhibitors of the enzyme. The IC_{50} values of these compounds range from 17 to 270 nM (in 1 mM phosphate), with 9-(3,4-dichlorobenzyl)-9-deazaguanine being the most potent inhibitor. X-ray analysis explained the role of the aryl groups and revealed the rearrangement of hydrogen bonds in the binding of the 9-deazaguanines in the active site of PNP relative to the binding of the 8-aminoguanines that results in more potent inhibition of the enzyme.

Introduction

Recent advances in X-ray crystallographic techniques, computer graphics, and related fields have resulted in a significant increase in the number of protein structure determinations and a decrease in the average time required to perform these determinations. Since the time required for structure analysis is now compatible with the needs of the pharmaceutical industry, the use of such structural information in drug design will become increasingly more common. Advances in computer hardware and computational methods are expected to impact molecular modeling by enabling the computational chemist to address more complex problems of small molecule protein interactions with a greater degree of accuracy. Although much attention has been focused on the concept of drug design based on crystallographic and modeling methods, few definitive examples of the application of this technique have appeared in the literature.[1-3] As the structures of more and more target macromolecules become available, the need for devising techniques to utilize structural data becomes even more apparent. Unquestionably, structural information in combination with graphical methods for displaying accessible volume, electrostatic potential, and active-site hydrophobicity can aid in drug design. Further enhancement in structure-based drug design is expected from methods that can accurately evaluate a target molecule in terms of binding geometry, binding affinity,

and binding-induced changes in protein conformation. Accurate prediction of binding affinities is currently not routinely possible, although significant advances have been made using free energy perturbation techniques.[4,5] Progress has also been made in the computational determination of the binding geometry of ligands associated with macromolecular receptors, and a number of "docking" algorithms have appeared recently that address this issue.[6-10] Recently, we have developed Monte Carlo-based conformational searching methods that, in combination with energy minimization, accurately predict the ligand binding conformations that are observed in the crystal structures of enzyme/inhibitor complexes.[11]

In this paper, we report the use of crystallographic and modeling methods for the design of competitive inhibitors of purine nucleoside phosphorylase (PNP, purine nucleoside: orthophosphate ribosyltransferase, EC 2.4.2.1), an enzyme that catalyzes the reversible phosphorolysis of purine ribonucleosides and 2'-deoxyribonucleosides to the free base and ribose-α-1-phosphate or 2-deoxyribose-α-1-phosphate (Figure 1).

The enzyme has been purified from a variety of sources including human erythrocytes,[12,13] placenta,[14] granulocytes,[15] bovine spleen,[16] bovine brain,[17] rabbit liver,[18] chicken liver,[19,20] bacteria,[21] and malarial parasites.[22] PNPs from most mammalian sources appear to be trimeric,[23-27] although both trimeric[12,28,29] and dimeric[30] quaternary structures have been proposed for the human enzyme. Human PNP has been sequenced[31] and has a calculated molecular mass of 32,000 Da/subunit.

Interest in PNP as a drug target arises from its ability to rapidly metabolize purine nucleosides and from the relationship between PNP deficiency and certain immunological diseases.[32-34] The high level of PNP activity in vivo[35] suggests that the chemotherapeutic potential of

---

* To whom correspondence should be addressed.
† BioCryst Pharmaceuticals, Inc.
‡ Southern Research Institute.
§ University of Alabama at Birmingham.
∥ CIBA-GEIGY Corp.
⊥ Present address: Gensia Pharmaceuticals, Inc., 4575 Eastgate Mall, San Diego, California 92121.
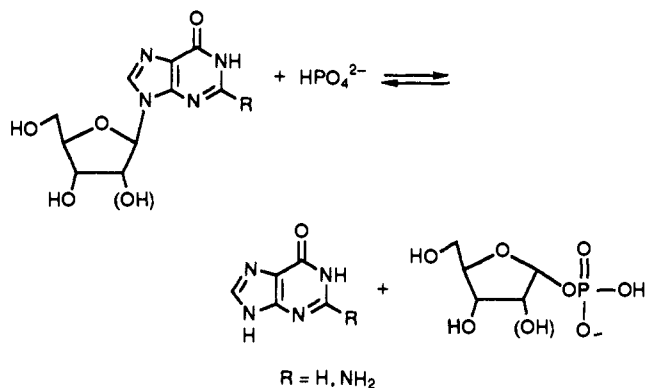⊕ Present address: Department of Biochemistry, Cornell University, 207 Biotechnology Building, Ithaca, New York 14853.

R = H, NH₂

Figure 1.

Figure 2.

certain purine nucleoside analogs may be severely compromised by PNP metabolism. These include the potential anticancer agents 2'-deoxy-6-thioguanosine, 2'-deoxy-6-thioinosine, and the anti-AIDS drug 2',3'-dideoxyinosine. Hence, the combination of a PNP inhibitor and these purine nucleoside analogs may prove to be more efficacious than the nucleoside alone. PNP inhibitors by themselves may have potential therapeutic value based on the finding that patients lacking PNP activity exhibit severe T-cell immunodeficiency while maintaining normal or exaggerated B-cell function.[32] This profile suggests that PNP inhibitors might be useful in the treatment of T-cell proliferative diseases, such as T-cell leukemia or T-cell lymphoma, in the suppression of the host vs graft response in organ transplant patients, and in the treatment of T-cell-mediated autoimmune disease such as rheumatoid arthritis and lupus. Despite the potential benefits of PNP inhibitors and despite the large number of PNP inhibitors that have been synthesized to date,[36,37] no compound has yet reached clinical trials. One problem is the potency of the membrane-permeable compounds thus far prepared. Although potencies for the best compounds have a higher affinity than the natural substrate (10–100X), T-cell immunotoxicity is expected to occur only with very tight binding inhibitors because of the high in vivo PNP activity and competition with substrates.[35] Hence, we determined the structure of human PNP, using X-ray crystallography,[38] and have utilized these results in combination with computer-assisted molecular modeling to design new highly-potent inhibitors of this key enzyme.[3]

Once the structure of PNP was known, a scheme was devised in which we utilized both inhibition data and X-ray crystallography for the evaluation of our target compounds and a combination of these data and molecular modeling for the design of the next round of inhibitors. A flow chart describing the overall strategy is shown in Figure 2. Ideas for new compounds resulted from the consideration of crystallographic data, computer modeling, and synthetic feasibility. Proposed compounds were screened by modeling the enzyme/inhibitor complexes using interactive computer graphics[39] and molecular mechanics-based molecular energetics using the AMBER force field.[40,41] Monte Carlo/Energy Minimization techniques[42] were employed to sample the conformational space available to potential inhibitors such as acyclovir diphosphate[43] docked into the PNP active site and evaluate them in terms of their potential binding geometries. Qualitative evaluation of the enzyme/inhibitor complexes using molecular graphics aided in prioritizing structures for chemical synthesis. The
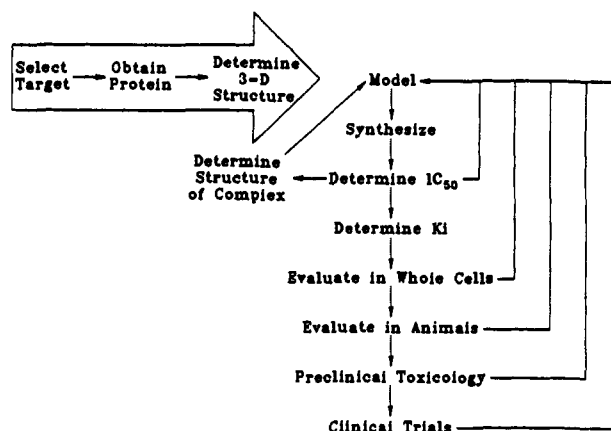
resulting compounds were evaluated by both determination of the IC_{50} values and X-ray diffraction analysis using difference Fourier maps (Figure 3).

Prior to this work, a number of PNP inhibitors had been identified by several investigators.[36,37] Probably the first significant inhibitor studied was 8-aminoguanine with a K_i of 0.8 μM against the human erythrocytic (HE) enzyme.[44] The only modification of 8-aminoguanine that improved its activity was substitution at the 9-position by aromatic groups attached through a methylene group. 8-Aminoguanines with a phenyl group directly attached to N-9, or attached through an ethylene group, were much less inhibitory.[45] While our work was in progress, other investigators reported that both the 2- (K_i = 0.067 μM, IC_{50} = 0.17 μM) and 3-(thienylmethyl) (IC_{50} = 0.085 μM) groups yielded significantly better inhibitors than the benzyl group (K_i = 0.2 μM).[37] Although, quite logically, a number of ribonucleoside analogs of inosine and guanosine have been investigated, none of them is as potent as the 9-(thienylmethyl)-8-aminoguanines. The best nucleoside analog reported to date is 5'-deoxy-5'-iodo-9-deazainosine (K_i[HE] = 0.18 μM).[46] Furthermore, both hypoxanthine and guanine bind more tightly than their ribonucleosides.

By far the most potent inhibitor reported prior to our work was acyclovir diphosphate, a metabolite of the antiviral agent acyclovir.[43] This compound has a K_i(HE) of 8.7 nM, but only in 1 mM phosphate buffer. The K_i in 50 mM phosphate buffer is 510 nM, indicating that it also competes with phosphate, the second substrate. It is not likely to be a serious drug candidate because it cannot penetrate cells intact and is unstable extracellularly, both metabolically and chemically. Furthermore, when generated intracellularly, it is further phosphorylated to the triphosphate which is not a good inhibitor of PNP, but does have effects on DNA synthesis that would preclude its use as a PNP inhibitor. The more recently reported[47] phosphonate analog, 9-(5,5-difluoro-5-phosphonopentyl)-guanine, is a potent inhibitor (K_i = 18 nM) and is stable, but must be given at 100 μM to show effects in whole cells.[48] Since calculations based on the amount of PNP in human cells and the K_m of the natural substrates suggest that an inhibitor capable of significantly affecting the T-cell branch of the immune system must have a K_i of ≤10 nM,[35] we undertook to design potent membrane-permeable inhibitors based on our knowledge of the three-dimensional structure of the active site of PNP.[3,38] In this report, we describe our work on 9-(arylmethyl) derivatives of 9-deazaguanine.
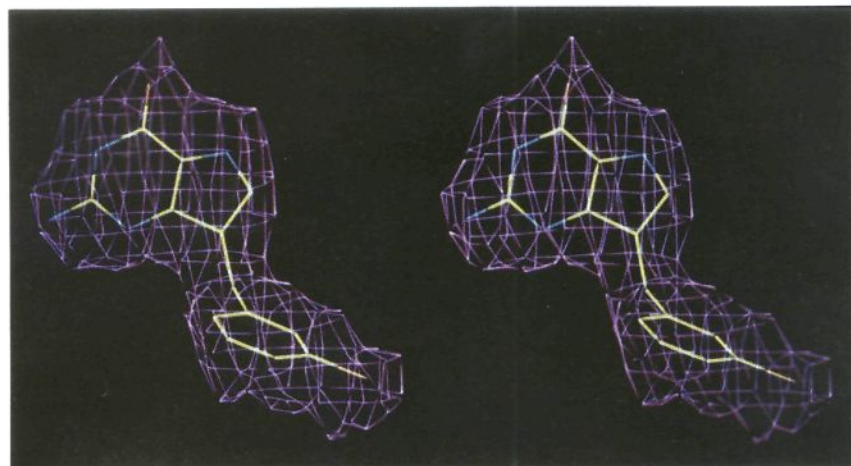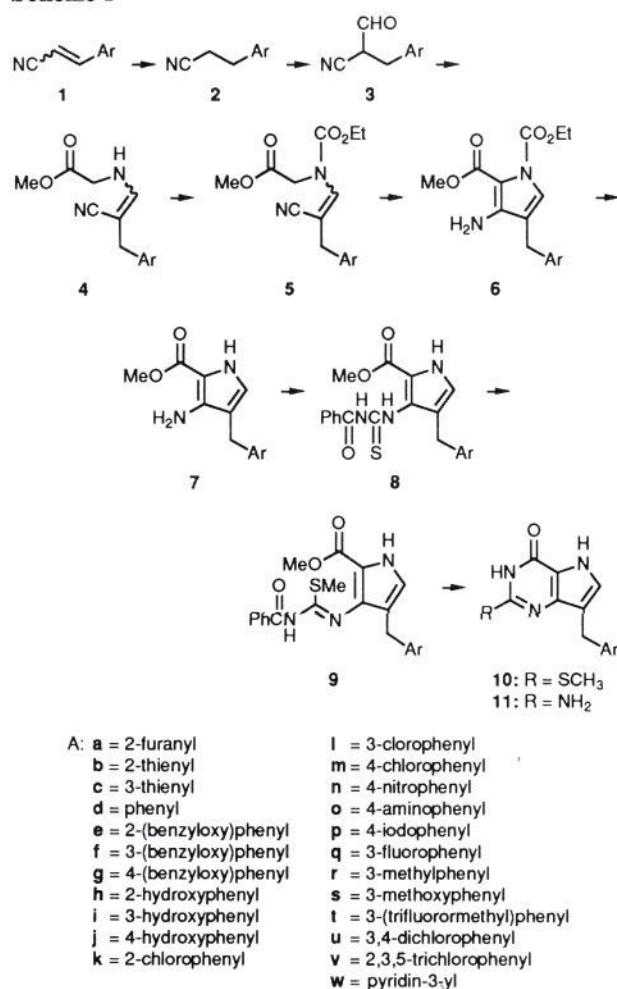
Figure 3. Difference Fourier map of 9-(3-chlorobenzyl)-9-deazaguanine bound in the active site of PNP.

Scheme I

A:
a = 2-furanyl
b = 2-thienyl
c = 3-thienyl
d = phenyl
e = 2-(benzyloxy)phenyl
f = 3-(benzyloxy)phenyl
g = 4-(benzyloxy)phenyl
h = 2-hydroxyphenyl
i = 3-hydroxyphenyl
j = 4-hydroxyphenyl
k = 2-chlorophenyl

l = 3-clorophenyl
m = 4-chlorophenyl
n = 4-nitrophenyl
o = 4-aminophenyl
p = 4-iodophenyl
q = 3-fluorophenyl
r = 3-methylphenyl
s = 3-methoxyphenyl
t = 3-(trifluorormethyl)phenyl
u = 3,4-dichlorophenyl
v = 2,3,5-trichlorophenyl
w = pyridin-3-yl

Chemistry

9-Deaza-9-substituted guanines 11 were prepared by an adaptation of a literature procedure for other 9-deazapurines (Scheme I).[49-52] Most of the requisite 3-aryl- and heteroarylpropenenitriles (1), prepared by the condensation of the appropriate aldehyde with cyanoacetic acid,[53] were reduced to the corresponding propanenitriles 2 catalytically (Pd/C) (Ar = a–c, m, o, q, r–v), by treatment with Mg in methanol[54] (Ar = e–g), or by NaBH₄ reduction

(Ar = **w**).[55] 4-Iodobenzenepropanenitrile (**2p**) was prepared from 4-nitrobenzaldehyde which was condensed with cyanoacetic acid to give 4-nitrobenzenepropanenitrile (**1n**). Catalytic hydrogenation of **1n** gave 4-aminobenzenepropanenitrile (**2o**), which was converted to **2p** by diazotization and treatment with KI. As an alternative to the condensation of an aldehyde with cyanoacetic acid, the appropriately substituted benzyl halide was used to alkylate methyl cyanoacetate in three cases. The resulting α-cyanocarboxylic ester was then saponified (NaOH) and the acid decarboxylated by heating in N,N-dimethylformamide to give the desired 3-substituted benzenepropanenitrile **2k**, **l**, and **m**.[56] 2-(Benzyloxy)benzenepropanenitrile (**2e**), 4-iodobenzenepropanenitrile (**2p**), and 2,3,5-trichlorobenzenepropanenitrile (**2v**) are the only substituted propanenitriles that have not been reported.

The next step of the synthetic sequence was the preparation of the 2-formylpropanenitriles **3**. The published procedure[57] for the preparation of this type of compound used sodium methoxide in benzene to remove a proton adjacent to the cyano group. The resulting anion was then treated with ethyl formate to give the desired 2-formylpropanenitriles in extremely poor yields. We found, however, that treatment of the 3-aryl- and heteroarylpropanenitriles **2** with sodium hydride in THF followed by the addition of ethyl formate in most cases gave 65–75% initial conversion to the desired 2-formylpropanenitriles (**3**). We also found that multiple additions of disproportionately large quantities of NaH and ethyl formate were required to drive the reaction to completion, and therefore it was much simpler and more expedient to carry out the reaction on a larger scale using excess nitrile and to accept the 65–75% conversion. Yields of **3** were usually greater than 90% based upon consumed nitrile. Unreacted nitrile **2** present in the crude reaction product was inert in the next step and could easily be recovered by column chromatography.

The rate and the extent of the conversion of the 3-aryl- and heteroarylpropanenitriles **2** to the formyl derivatives **3** depends upon the nature of the aromatic group and its substituents. Electron donating substituents such as -OR on a phenyl ring greatly retard the conversion. For example, in the cases of **2e** and **2g**, little conversion was achieved unless an excess of reagents was added and the reaction mixture heated at reflux. In contrast, electron-withdrawing substituents such as halogens speed up the

reaction and these propionitriles give high yield of the formyl derivatives (**3k, l, m**) at room temperature.

The reaction of 2-formylpropanenitriles **3** with methyl glycinate hydrochloride in aqueous methanol at room temperature in the presence of sodium acetate readily afforded the enaminonitriles **4** in 60–70% overall yields as a mixture of cis and trans isomers. The ^{1}H-NMR spectra of **4** are consistent with the enamine structure in that they showed two sets of doublets ranging from δ 3.30–4.0 (CH_2-NH) and at δ 6.32–6.98 (>C=CH) that collapsed into singlets upon D_2O exchange of the NH protons at δ 4.73–6.82. Furthermore, their infrared spectra exhibited a single band in the range from 3325–3400 cm^{-1} consistent with bands for enamines. Our data is also consistent with that on similar enamine precursors of 9-deazapurines.[49,51]

According to the literature,[58] blocking of the NH group of enaminonitriles for the effective ring closure to the desired 3-aminopyrroles (**4–6**) can be achieved by treatment with ethyl chloroformate and 1,5-diazabicyclo[4.3.0]-non-5-ene (DBN) in dichloromethane. Our initial efforts to reproduce this work using the enaminonitriles **4e–g,k,m** and ethyl chloroformate (1.5 equiv) in the presence of DBN (2.0 equiv) at 0 °C for 4–5 h resulted in the formation of a mixture of carbamate intermediates **5** (~55%), N-protected pyrroles **6** (~25%), and unreacted starting material **4** (~20%). However, compounds **4** react with 1.5 equiv of ethyl chloroformate and 3.0 equiv of DBN first at 0 °C for 1 h and then 16 h at room temperature to give **6** in almost quantitative yield in one step. Only a small amount of pyrrole **7** is formed as a result of removal of the carbethoxy group by DBN. The mixture of compounds **6** and **7** could then be decarbethoxylated by treatment with sodium carbonate (1–2.5 equiv) in methanol. The large scale preparations of **7** from **4** were easily carried out without purifying **6**. Although compounds **4** and **7** have the same molecular ion, they are easily distinguished by their infrared spectra. Compounds **4** show a moderately strong C≡N band in the 2210–2240 cm^{-1} region that is absent in **7**. The structures of the 3-aminopyrroles **7** were assigned on the basis of their ^{1}H-NMR spectra, mass spectral data, and elemental analyses. These pyrrole derivatives showed broad singlets at δ 10.46–10.66 and doublets at δ 6.41–6.57 ($J_{H-5,NH}$ = 3.2–3.6 Hz), typical signals for the NH and H-5 of similar aminopyrroles.[51]
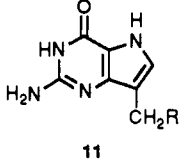
The obvious route for the construction of guanine analogs seemed to be the direct cyclization of **7** with guanidine, analogous to similar cyclizations of a wide variety of cyclic enaminonitriles to the corresponding fused 2-aminopyrimidine systems.[59] Unfortunately, the attempted reaction of 3-amino-4-substituted pyrroles **7** with guanidine hydrochloride and guanidine carbonate in boiling ethanol or methoxyethanol was unsuccessful even after 3 days of heating. The synthetic route finally adopted[51,60,61] was the treatment of **7** with benzoyl isothiocyanate in dichloromethane at room temperature. This reaction afforded the desired 2-(carbomethoxy)-3-[[N-benzoyl(thiocarbamoyl)]amino]-1H-pyrroles **8** in 85–99% yields. S-methylation of **8** was then carried out by treatment with methyl iodide in the presence of DBN in dichloromethane to give **9** in 83–99% yields after column chromatographic purification. Both **8** and **9** could be obtained as highly pure materials that were readily identifiable by their ^{1}H-NMR spectra and elemental analyses. The ^{1}H-NMR spectra of the methyl 3-[[[(benzoylamino)methylthio]methylene]amino]-4-benzyl-1H-

pyrrole-2-carboxylates show methyl singlets in the range of δ 2.42–2.53. The pyrrole H-5's are still seen as doublets in the range of δ 6.76–6.95 ($J_{H-5,NH}$ = 2.8–3.2 Hz) and the pyrrole ring NH's are seen as broad singlets in the range of δ 11.98–12.06, thus affording conclusive evidence for the S-methylation of **8**.

Treatment of **9** with methanolic ammonia (presaturated at 0 °C) in a glass-lined stainless steel bomb heated at 95–110 °C for 20–24 h gave a mixture of 7-(arylmethyl)-1,5-dihydro-2-(methylthio)-4H-pyrrolo[3,2-d]pyrimidin-4-ones (**10**, 15–30% yield) and the desired 9-deaza-9-substituted guanines (**11**, 45–55% yield) along with benzamide. Attempts to convert **10** into **11** under ammonolytic conditions identical with those leading to **11** were unsuccessful. This finding was consistent with the previously observed[51] lack of reactivity of a similar (methylthio)-substituted 9-deazapurine toward ammonia, demonstrating that **10** was not an intermediate in the formation of **11**. Although the formation of 2-(methylthio) byproduct **10** could not be eliminated, its formation was minimized by rapid heating of the bomb containing the reaction mixture to a temperature of 95–110 °C. Since early tests showed that these methylthio byproducts were not good PNP inhibitors, few of these compounds were isolated and purified. During our large-scale synthesis of these 9-deaza-9-arylguanines (10–20-g scale), we found it to be advantageous to use a concentrated solution of compounds **9** in methanolic ammonia and to cool the bomb for 6–7 h prior to opening. This procedure allowed us to obtain almost half of the desired **11** as a pure amorphous solid. The filtrate could then be evaporated to give a solid, which was washed with ether and methanol and then extracted into ethanol (Soxhlet extractor) to obtain additional quantities of compound **11**.

Discussion of Results

We selected the 9-deazaguanines for our initial work because we did not identify any interaction of N-9 of the guanine analogs studied with any residue in the purine binding site of PNP. In addition, 5'-deoxy-5'-iodo-9-deazainosine was the best nucleoside inhibitor of PNP (see above), and an X-ray study of its complex with PNP was encouraging.[62] In fact, 9-deazainosine itself binds 15–20 times more tightly than inosine.[46] Since, at the time this study was undertaken, 8-amino-9-benzylguanine was the most potent known membrane-permeable inhibitor of the enzyme,[45] we prepared 9-benzyl-9-deazaguanine (Table I). This compound (**11d**) proved to be significantly more potent than 8-amino-9-benzylguanine, and an X-ray study of its complex with PNP showed the "herringbone" interaction[63] of its phenyl ring with the phenyl rings of Phe-159 (from the adjacent subunit) and Phe-200 indicating near maximal interaction with the hydrophobic pocket of PNP and provided for the first time an explanation for the potency of the 9-(arylmethyl) analogs. It also confirmed the fact that potent inhibitors did not have to have an amino group in the 8-position of the heterocyclic ring, although it was not immediately evident that such a substitution was actually detrimental in the case of 9-deazapurines (see Table II). Only after a comparison of the IC_{50} values of the guanine/8-aminoguanine and 9-deazaguanine/8-amino-9-deazaguanine pairs did this fact become apparent, leading to an X-ray examination of the four complexes of the thienylmethyl compounds with PNP (Figure 4).

Table I. Inhibition of PNP[a]

11

no.	R	IC$_{50}$ (nM) 1 mM PO$_4$	50 mM PO$_4$	ratio[b]
u	3,4-dichlorophenyl	17 ± 7	250	15
l	3-chlorophenyl[c]	20 ± 7	150 ± 2	8
b	2-thienyl[c]	21 ± 4	150 ± 40	7
p	4-iodophenyl	23	270	12
q	3-fluorophenyl	24	220	9
c	3-thienyl[c]	25	80	3
m	4-chlorophenyl[c]	25 ± 3	380 ± 30	15
w	pyridin-3-yl	25 ± 2.8	190 ± 42	8
t	3-(trifluoromethyl)phenyl	36 ± 12	190 ± 39	5
d	phenyl[c]	51 ± 12	210 ± 30	4
r	3-methylphenyl	57	270	5
i	3-hydroxyphenyl[c]	70 ± 20	274 ± 120	4
s	3-methoxyphenyl	82	660	8
a	2-furanyl	83	313 ± 66	4
k	2-chlorophenyl[c]	120 ± 40	2520 ± 390	21
f	3-(benzyloxy)phenyl[c]	147 ± 70	740 ± 85	5
v	2,3,5-trichlorophenyl	240	10000	
j	4-hydroxyphenyl[c]	260	2300	9
h	2-hydroxyphenyl[c]	270	2000	7
ATG[d]		160	160	1

[a] Calf spleen enzyme. Values without standard deviations are averages of results of two determinations that did not differ by more than 15%. Other values are for results of three or more determinations and are shown as mean ± standard deviation. The low solubility of many of the compounds may have contributed to variations at the higher concentrations. Compounds a–d were also evaluated against the enzyme from human erythrocytes (Sigma Chemical Co.) in 50 mM phosphate. The ratios of IC$_{50}$ CS/IC$_{50}$ HE ranged from 1.2 to 5.4, but the relative potencies were about the same as those obtained with the calf spleen enzyme. [b] IC$_{50}$ (50 mM PO$_4$)/IC$_{50}$ (1 mM PO$_4$). [c] Structure of PNP complex determined by X-ray crystallography. [d] 8-Amino-9-(2-thienylmethyl)guanine.[37]

Table II. PNP Inhibitors: Effects of 8-Amino Substitution

9-substituent	IC$_{50}$ (μM)[a,b] G	8-AG	ratio[c]	IC$_{50}$ (μM)[a] 9-DG	8A-9DG	ratio[d]
2-thienylmethyl	11	0.16	0.015	0.03	1.0[e]	33
3-thienylmethyl	–	0.085	–	0.067	0.63	10
3-methyl-2-thienylmethyl	47.6	4.05	0.08	–	–	–
2-furanylmethyl	17.9	0.25	0.014	0.057	0.75	14
benzyl	29.6	0.47	0.017	0.085	0.85	10
3-pyridin-3-yl	57	21.9	0.38	0.16[f]		

[a] Human erythrocytic PNP (50 mM phosphate). [b] Data from ref 37. [c] IC$_{50}$ 8-AG/IC$_{50}$ G. [d] IC$_{50}$ 8-A-9-DG/IC$_{50}$ 9-DG. [e] Data from U.S. Patent 5,061,707. [f] Calf spleen PNP (50 mM phosphate).

This analysis of the structures of these four complexes revealed two different hydrogen bonding schemes, one for the guanine and 8-aminoguanine analogs and a second one for the 9-deazaguanine and 8-amino-9-deazaguanine analogs. In the first case, the amino group of Asn-243 forms hydrogen bonds with O(6) and N(7) of the purine. Asn-243 is anchored in position by a hydrogen bond with Thr-242. The 8-aminoguanine analog binds to PNP more tightly than the unsubstituted compound because of an additional hydrogen bond between the 8-amino group and the hydroxyl of Thr-242. The shift of Asn-243 in the direction of the pyrimidine ring relative to the pyrrole ring of the 9-deazaguanines was clearly seen in the difference electron density maps for the 9-deazaguanines, indicating that, in the second case, Asn-243 rearranges to form a more optimal hydrogen bond between O(δ) of Asn-
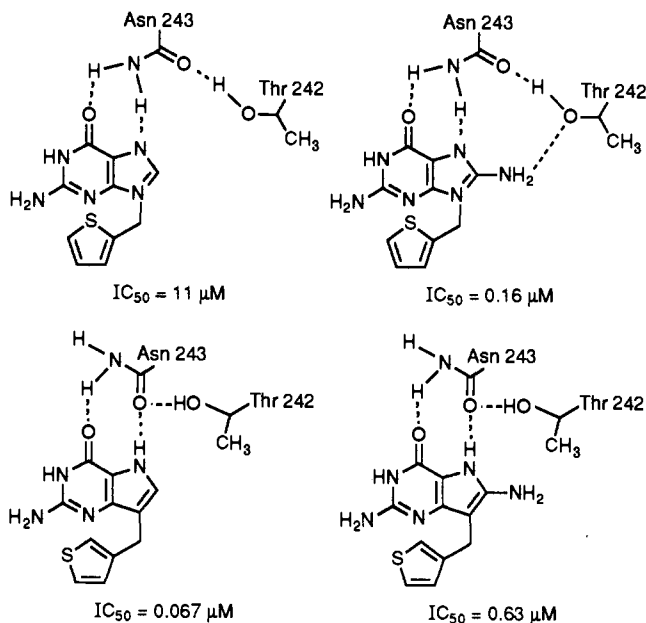
Figure 4.

243 and N(7) of the purine, which in the 9-deazaguanine analogs bears a hydrogen, while the hydrogen bond between the amino group of Asn-243 and O(6) of the 9-deazapurine is maintained. This rearrangement of hydrogen bond donors and acceptors near N(7) results in a shift in the position of O(δ) of Asn-243 of about 2.5 Å with a corresponding shift in Thr-242 to maintain a hydrogen bond with Asn-243. In the case of the second hydrogen bonding scheme, the hydroxyl of Thr-242 is no longer available to hydrogen bond to an 8-amino group and, in fact, the threonine methyl group is now in close contact with the 8-amino group. Although the hydrogen atom positions obtained from crystallographic data must be calculated and the hydrogen bonding scheme derived by inference, the hydrogen bonding schemes shown in Figure 4 are consistent with all available structural and biochemical data, and provide the only logical explanation for the beneficial effect of the 8-amino modification on guanine analogs and its detrimental effect on 9-deazaguanine analogs.

Concurrently with crystallographic and kinetic studies, inhibitor complexes were evaluated using molecular mechanics-based energy minimization. Because of a conformational change that resulted from inhibitor binding, initial modeling studies based on coordinates of the native enzyme were not useful in predicting new inhibitors. However, modeling studies based on coordinates that incorporated the conformational change reliably predicted the herringbone packing observed in the X-ray crystal structures of 9-(arylmethyl)-substituted inhibitors complexed with PNP. These structures were in turn used to explore possible substitution patterns for the aromatic groups as well as other modifications that might lead to more tightly binding PNP inhibitors. The results of the modeling studies were combined with experimental data derived from crystallographic and biological studies to produce a priority ranking for compound synthesis.

An understanding of the enhanced binding of the 9-deazaguanines led us to concentrate our efforts on modification of the 9-benzyl group of 11d. Crystallographic analysis of the complexes of some of these derivatives (e.g., the 2-, 3-, and 4-chlorobenzyl compounds 11k, l, and m) revealed significant displacements of them
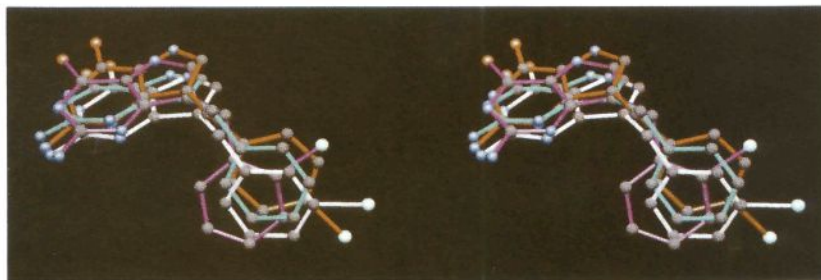
Figure 5. Ball and stick models of 9-(2-chloro-[purple], -3-chloro-[white], and -4-chlorobenzyl)[orange]-9-deazaguanines compared to 9-benzyl-9-deazaguanine [turquoise] bound in the active site of PNP.

Table III. Inhibition Constants for Some Inhibitors of PNP[a]

| | K_i (nM) | | | |
| | inosine[b] | | PO$_4$[b] | |
inhibitor	50 mM PO$_4$	1 mM PO$_4$	K_{ii}	K_{is}
8-amino-9-(2-thienyl-methyl)guanine	90 (C)[c]	45 (C)	200	270
9-(2-thienylmethyl)-guanine	–	2000 (C)	6000	11000
9-(2-thienylmethyl)-9-deazaguanine (11b)	–	15 (C)	34	14
9-benzyl-9-deazaguanine (11d)	100 (C)	12 (C)	45	30

[a] Calf spleen. [b] Variable substrate. [c] C = competitive.

in the active site that appeared to result from close contacts between the inhibitor and the sulfate ion that occupies the phosphate binding site (Figure 5). Therefore, we assayed these and other inhibitors at both 1 and 50 mM phosphate. The results listed in Table I show that the IC$_{50}$ (50 mM) values are consistently larger than the IC$_{50}$ (1 mM) values, in some cases by as much as 20-fold. Other inhibitors such as 8-aminoguanosine and 8-amino-9-(2-thienylmethyl)guanine (ATG) show no difference. In the case of 8-aminoguanosine, the result may be due to the hydrogen bond between the phosphate and O(3′). Since the concentration of phosphate in intact cells is about 1 mM, we have based our conclusions on the data collected at this concentration, although we continued to assay at 50 mM phosphate also to permit comparisons with literature data.

The most potent compound of this series is the (3,4-dichlorobenzyl)-9-deazaguanine (11u), although most of the other halo-substituted compounds (11l, m, p, q, and t) are only 2- to 3-fold less potent. Even the relatively large iodo group at the 4-position (11p) does not interfere with binding. In contrast, the 4-hydroxyl compound (11j) gives an unfavorable interaction and is more than an order of magnitude less potent. Substitution at the 2-position of the phenyl ring is also detrimental and an X-ray study of the complexes showed that both the deazapurine and the phenyl ring are displaced from the positions they occupy in the PNP/9-benzyl-9-deazaguanine complex. The aromatic ring is deeper in the hydrophobic pocket formed by Phe-159 and Phe-200. Since the functional form of hydrophobic interactions is linear,[64] the hydrophobic interaction of the 2-chloro compound 11k must be greater than that of the 3- and 4-chloro compounds 11l and m. Thus, the 6-fold higher IC$_{50}$ value (a reflection of decreased binding) of 11k must be due primarily to the displacement of the 9-deazaguanine moiety from its optimal binding position resulting in a weakening of its hydrogen bonding interactions with the amino acid side chains making up

the purine binding site. This 2-dimensional displacement is clearly visible in Figure 5. Both the halogens and the hydroxyl group on the phenyl ring are all oriented away from the hydrophobic pocket into the aqueous environment. The sulfur of the thienylmethyl group (11b,c), on the other hand, is oriented into the hydrophobic pocket. In general, as expected, the more hydrophobic aromatic groups provide the more potent inhibitors unless steric factors are unfavorable. The differences between the top 11 compounds in Table I (u–r), even though reproducible, are probably not significant. These compounds are, however, significantly better than the last eight compounds (i–h). The poorest inhibitor, 9-(2-hydroxybenzyl)-9-deazaguanine (11h) is 22.5 times less potent than the best inhibitor (11u).

The K_i values for two of these inhibitors (11b,d) have been determined along with those of 9-(2-thienylmethyl)-guanine and its 8-amino derivative (Table III). These compounds are competitive inhibitors with respect to inosine. Several of these 9-deazaguanines were inhibitory to the growth of CCRF-CEM cells in the presence of 5.6 μM 2′-deoxyguanosine, having IC$_{50}$ values of 0.4–0.7 μM, whereas the 8-amino-9-benzyl and 8-amino-9-(3-thienyl-methyl)-9-deazaguanines were ineffective at 20 μM. Some of the effective 9-deazaguanines were also shown to elevate plasma inosine and to increase the half-life and area under the curve (AUC) of ddI in Lewis rats.[62]

Conclusions

At the beginning of these studies, equal weight was given to both modeling and traditional medicinal chemical approaches. The reasons for the selection of the first compounds proposed for synthesis were outlined above. Initial molecular modeling studies involved positioning potential inhibitors in the PNP binding site with the aid of molecular graphics followed by energy minimization of the complex. The resulting structures qualitatively appeared to be quite reasonable in terms of nonbonded contacts, hydrogen bonding, etc. However, subsequent crystallographic studies on several of the 9-(arylmethyl)-9-deazapurine/PNP complexes yielded results inconsistent with the modeled structures. Two likely reasons for the failure of the initial modeling procedures to predict the correct structure were (1) even though molecular mechanics-based energy minimization of arbitrary conformers of potential inhibitors docked to the PNP binding site consistently resulted in structures with the purine ring correctly positioned, inadequate sampling of the conformational space available to the 9-(arylmethyl) substituents resulted in inaccurate positioning of these side chains and (2) the calculations were based on the coordinates for the

Table IV. Monte Carlo/Energy Minimization of Inhibitors in the PNP Binding Site
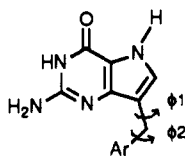
	predicted[a]		observed[b]	
Ar	θ1	θ2	θ1	θ2
phenyl	−75	141	−73	134
2-chlorophenyl	−70	124	−101	145
3-chlorophenyl	−84	149	−72	102
4-chlorophenyl	−44	89	−73	102
3-thienyl[d]	−67	144	−90	144

[a] Torsion angles for the low energy conformation that most closely resembled the one observed crystallographically. [b] Torsion angles derived from Fourier difference maps. [c] Estimated errors in predicted and observed torsion angles are about 10°. Errors in the observed torsion angles result from experimental errors in calculating and fitting the difference electron densities. Errors in the predicted values result from uncertainties in the model and in the force constants used for energy minimization. [d] 8-Amino-9-(3-thienylmethyl)guanine.

native PNP structure that did not adequately represent the binding site in the PNP/inhibitor complexes. The modeling procedure was then changed by replacing the coordinates for the active site model with coordinates from the refined PNP/guanine complex. In addition, conformational searching using the Monte Carlo calculations[11,42] mentioned above was incorporated into the energy minimization procedure. The new protocol was then used to evaluate several 9-(arylmethyl)-9-deazaguanine analogs with the results shown in Table IV. The agreement between predicted and observed torsion angles in Table IV is actually quite good considering the past record of success for modeling methods in predicting the binding geometry of enzyme inhibitors. One should assume estimated errors of around 10° in both predicted and observed torsion angles. Even errors of 20–30° would still show most of the correct aromatic interactions.

As discussed above, substitution of the 9-deazaguanines at the 8-position by an amino group unexpectedly *decreased* the potency of them by about 2 orders of magnitude in contrast to the *enhancement* of potency of guanines by about the same amount—a truly large difference of 3–4 orders of magnitude. A detailed analysis of the crystallographic data on the pairs of complexes (see above) showed that a rearrangement of hydrogen bonding between the 9-deazapurine and Asn-243 prevented the active site residues from satisfying all of the hydrogen bond donors, i.e., the 8-amino group and, in fact, causes the methyl group of Thr-242 to come in close contact with the 8-amino group resulting in a decrease rather than an increase in binding to the active site. The ability of X-ray crystallographic analysis to provide a lucid and convincing explanation for this apparent anomaly demonstrates the power of this approach in understanding small molecule–protein interactions and ultimately in drug design.

During the work described in this paper, we did not *routinely* predict in advance of chemical synthesis and subsequent X-ray crystallographic analysis the geometry of potential PNP inhibitors. Even so, molecular graphics and molecular mechanics-based molecular modeling studies were of considerable utility. We used the crystallographic data to explain the observed inhibition data and to develop modeling procedures that agree with experimentally determined active site structures. The most

important benefit derived from the crystallographic data was a more complete understanding of the PNP/inhibitor complex that led to the optimization of the initial compounds through modifications consistent with the active site structure. The most important conclusions from computer modeling studies were (1) conformational changes that occur during substrate/inhibitor binding are difficult to predict but must be manually incorporated into subsequent modeling studies in order to accurately predict inhibitor binding geometry and (2) conformational searching techniques, such as Monte Carlo simulations, are necessary to avoid local energy minima and accurately predict inhibitor binding geometry. Using this approach, modeling studies suggested further structural modifications consistent with accessible volume and the geometrical constraints of active site amino acid residues. These studies, for example, suggested appropriate substituents and positions for substitution on the 9-(arylmethyl)-9-deazaguanines reported herein. Subsequently, the crystallographic and theoretical studies suggested new classes of compounds that will be described in future publications, e.g., 9-cycloaliphatic-9-deazaguanines and 9-(arylmethyl)-9-deazaguanines substituted at the benzylic carbon.
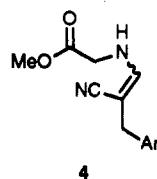
Experimental Section

Chemistry. All evaporations were carried out in vacuo with a rotary evaporator or by short-path distillation into a dry ice/acetone-cooled receiver under high vacuum. Analytical samples were normally dried in vacuo over P_2O_5 at room temperature for 16 h; high-melting compounds were dried at 110 °C. Analtech precoated (250 μm) silica gel G(F) plates were used for TLC analyses; the spots were detected by irradiation with a Mineralight and absorption of iodine vapor. All analytical samples were homogeneous by TLC. Melting points were determined by the capillary method with a Mel-Temp apparatus unless otherwise specified and are uncorrected. Purifications by gravity column and by flash chromatography[65] were carried out on Merck silica gel 60 (230–400 mesh) using the slurry method of column packing. The UV absorption spectra were determined in 0.1 N HCl (pH 1), pH 7 buffer, and 0.1 N NaOH (pH 13) with a Cary 17 spectrophotometer and a Perkin-Elmer UV-visible near-infrared spectrophotometer Model Lambda 9: the maxima are reported in nanometers (ε × 10^{-3} M^{-1} cm^{-1}). The ^{1}H-NMR spectra of all compounds were determined with a Nicolet/GE NT 300NB spectrometer operating at 300.635 MHz with tetramethylsilane as an internal reference. Chemical shifts (δ, ppm) quoted in the case of multiplets are measured from the approximate center. The mass spectra were obtained with a Varian-MAT 311A mass spectrometer in the fast-atom-bombardment (FAB) mode or the electron-impact (EI) mode. Where analyses are indicated only by symbols of the elements, analytical results obtained for those elements were within ±0.4% of the theoretical values. All solvates were confirmed by NMR. Infrared spectra were determined in pressed KBr discs with a Nicolet Model 10DX spectrophotometer; values are reported in reciprocal centimeters (cm^{-1}). Data on compounds 4, 6, 8, 9, and 11 are given in Tables V–IX. The following intermediates were purchased from Aldrich Chemical Co.: 2-furanpropenenitrile, benzenepropanenitrile, and 2-chlorobenzenepropanenitrile.

Synthesis of 3-Substituted Acrylonitriles 1. Standard Procedure. The synthesis of 3-(2-benzyloxyphenyl)propenenitrile will be described to illustrate a standard procedure by which the compounds (Ar = b,c,e,f,g,n,q,r–w) were prepared.

3-[2-(Benzyloxy)phenyl]propenenitrile (1e). A mixture of cyanoacetic acid (10.38 g, 122 mmol), 2-(benzyloxy)benzaldehyde (28.50 g, 134 mmol), ammonium acetate (500 mg), toluene (120 mL), and pyridine (65 mL) was refluxed for 44 h in a flask fitted with a Dean–Stark trap and condenser. After evaporation of solvents, a solution of the residue in CH_2Cl_2 was washed with H_2O, dried over Na_2SO_4, and evaporated. The crude product was purified by chromatography on a silica gel column ($CHCl_3$ eluent) to give 3-[2-(benzyloxy)phenyl]propenenitrile (1e) as a

Table V

4

no.	Ar	% yield	mp, °C	PM[a]
a	2-C₄H₃O	–	b	A
b	2-C₄H₃S	78	c	B
c	3-C₄H₃S	89	d	A
d	C₆H₅	89	67–71	C
e	2-BzlOC₆H₄	74.3	d	A
f	3-BzlOC₆H₄	89.8	c	A
g	4-BzlOC₆H₄	85	d	D
k	2-ClC₆H₄	78.6	90–92	A
p	4-IC₆H₄	81	d	A
q	3-FC₆H₄	88.8	c	D
r	3-MeC₆H₄	82.7	c	A
s	3-MeOC₆H₄	69	82–83	A
t	3-CF₃C₆H₄	87.4	d	A
u	3,4-Cl₂C₆H₃	73.4	77–79	A
v	2,3,5-Cl₃C₆H₂	84.9	110–111	E
w	3-C₆H₄N	65	b	E

^{a} Purification method: A, column chromatography on silica gel using CHCl₃ as the eluent; B, washed with cyclohexane and used in the next step without further purification; C, column chromatography on silica gel using CHCl₃/MeOH (95:5) as the eluent; D, used in the next step without purification; E, column chromatography on silica gel using CHCl₃/methanol (98:2) as the eluent. ^{b} Gum. ^{c} Oil. ^{d} Semisolid.

clear oil: yield 26.97 g (93.9%); ¹H-NMR spectrum of this compound indicated an ~2:1 ratio of trans to cis isomer; MS (EI) m/z 235 (M)⁺; IR 2214 (C≡N), 1612, 1599 (C=C); ¹H-NMR δ 5.09, 5.12 (s, 2, 2, CH₂), 5.40, 6.03 (d, d, 1, CHCN), 7.63, 7.66 (d, d, 1, ArCH=), 6.92–8.14 (m, 9, ArH). Anal. (C₁₆H₁₃NO) C, H, N.

4-Nitrobenzenepropenenitrile (1o). A mixture of cyanoacetic acid (12.76 g, 150.0 mmol), 4-nitrobenzaldehyde (24.60 g, 162.8 mmol), ammonium acetate (500 mg), toluene (140 mL), and pyridine (75 mL) was refluxed for 64 h in a flask fitted with a Dean–Stark trap and condenser. After evaporation of the solvents, a solution of the residue in CHCl₃ was filtered and washed with H₂O. The dried (Na₂SO₄) organic layer was evaporated, and the bright yellow-orange solid was recrystallized from benzene. The yellow solid 4-nitrobenzenepropenenitrile, obtained in 96% yield as a mixture of cis–trans isomers, was suitable for use as an intermediate without further purification.

2,3,5-Trichlorobenzenepropenenitrile (1v). The experimental procedure is essentially the same as described for 1e, yield (79.6%): mp 124–125 °C; MS (EI) 231 (M)⁺, 196 (231-Cl)⁺; IR (KBr) 2221 (CN), ¹H-NMR δ 6.7 (d, 2, CH₂, J₂,₃ = 18 Hz), 7.8 (d, 2, CH₂, J₂,₃ = 18 Hz), 8.0 (bs, 2, ArH). Anal. (C₉H₄NCl₃) C, H, N.

Synthesis of 3-Substituted Propanenitriles 2. The synthesis of 3-substituted propanenitriles 2 could be carried out by the reduction of the corresponding acrylonitriles by one of the following three methods:

(1) **Catalytic Hydrogenation Method.** The synthesis of 4-aminobenzenepropanenitrile (2o) from the acrylonitrile will be described to illustrate a standard procedure by which the compounds 2 (Ar = a–c,m,o,q–v) were prepared.

4-Aminobenzenepropanenitrile (2o). A partial solution of 4-nitrobenzenepropenenitrile (1o) (24.1 g, 138 mmol) in EtOH (800 mL) was hydrogenated at atmospheric pressure with 5% palladium-on-carbon catalyst. The initial reaction was exothermic and ice-bath cooling was required to prevent overheating. As soon as reduction of the nitro group was complete, a nearly colorless solution was obtained and external cooling was removed. Hydrogen consumption stopped after 9 h, and the volume was 106% of theory. After filtering off the catalyst and evaporating the solvent, a solution of the residual orange oil in CHCl₃/MeOH (99:1) was combined with a similar product from a previous pilot run and chromatographed on a silica gel column. Fractions

containing 2o of sufficient purity for use as an intermediate totaled 12.8 g (60.8%).

2,3,5-Trichlorobenzenepropanenitrile (2v). The experimental procedure is essentially the same as described for 2o, starting from 2,3,5-trichlorobenzenepropenenitrile (1o): yield 82%; mp 45 °C; MS (EI) 233 (M)⁺, 193 (233 – CH₂CN)⁺; IR (KBr) 2192 (CN); ¹H-NMR δ 2.9 (t, 2, CH₂), 3.1 (t, 2, CH₂), 7.6 (d, 1, ArH), 7.8 (d, 1, ArH). Anal. (C₉H₆NCl₃) C, H, N.

(2) **Magnesium Metal Reduction Method.** Synthesis of 3-[2-(benzyloxy)phenyl]propanenitrile (2e) from the acrylonitrile will be described to illustrate a standard procedure by which compounds 2 (e–g) were prepared.

3-[2-(Benzyloxy)phenyl]propanenitrile (2e). Magnesium turnings (99.2 g, 4.08 mol) were added in portions to a solution of 2-(phenylmethoxy)benzenepropenenitrile (1e, 24.00 g, 0.102 mol) in 2 L of absolute methanol. An oversized flask and an efficient ice/water cooling bath were required to control the foaming from the vigorous exothermic reaction. As much of the MeOH as possible was evaporated from the thick paste under aspirator vacuum. With cooling in an ice bath, ice cold 6 N HCl was added very slowly with cautious hand stirring until the magnesium salts were just dissolved, and a slightly turbid solution was obtained. The aqueous mixture was extracted with several portions of CHCl₃. The extract was washed by shaking with 0.1 N NaOH (100 mL) and H₂O (2 × 100 mL), dried (Na₂SO₄), and evaporated to give 1e as a clear dark oil: yield 23.2 g (96%). The oil was purified by vacuum distillation using a simple Claisen head: yield 18.2 g (75%); bp 152–154 °C/0.08 Torr. The distillate crystallized to a brittle white solid on standing, mp 45–46 °C. Portions of the solid were recrystallized from boiling cyclohexane and from EtOH/H₂O (2:1), but neither process raised the melting point: MS (EI) 237 (M)⁺, 146 (237 – CH₂O)⁺, 130 (237 – OCH₂)⁺; IR 2240 cm⁻¹ (CN); ¹H-NMR (DMSO-d₆) δ 2.75 (t, 2, CH₂CN), 2.87 (t, 2-CH₂CH₂CN), 5.15 (s, 2, OCH₂Ph), 6.93–7.52 (m, 9, ArH). Anal. (C₁₆H₁₅NO) C, H, N.
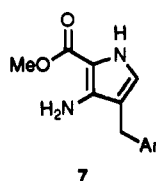
(3) **Sodium Borohydride Reduction Method.**[55] Only compound 2w was prepared by this method.

3-(3-Pyridinyl)propanenitrile (2w). A solution of 1w (242.7 g, 1.86 mol) in MeOH (3.0 L) and H₂O (750 mL) (4:1) was cooled in an ice bath and treated portionwise over several hours with a total of 5.6 mol of NaBH₄ pellets. The reaction mixture was cooled in an ice bath/salt bath, and glacial acetic acid was added with vigorous stirring at such a rate that the temperature was maintained below 15 °C. The reaction mixture was adjusted to pH 5, methanol (2 L) was added, and the mixture was allowed to stand overnight. The solvent was evaporated in vacuo, the residue was taken up in H₂O (800 mL), and the solution was extracted in portions with a total of 5 L of CHCl₃. The combined extract was dried (Na₂SO₄) and evaporated to give a clear oil (yield 195 g) that was purified by vacuum distillation to provide 153.8 g (62%) of material that was used directly in the next step, MS (FAB) m/z 132 (M + H)⁺.

4-Iodobenzenepropanenitrile (2p). A mixture of 4-aminobenzenepropanenitrile (2o) (12.82 g, 87.7 mmol) and concentrated H₂SO₄ (18.9 g, 193 mmol) in H₂O (85 mL) was cooled to −4 °C in an ice/salt bath, and the suspension was treated slowly with a solution of NaNO₂ (6.35 g, 98.1 mmol) in H₂O (30 mL) at such a rate that the internal temperature remained below −2 °C. Ten minutes after the last addition, solid urea (0.53 g, 8.8 mmol) was added to destroy excess nitrous acid. A cold solution of KI (20.38 g, 122.8 mmol) in H₂O (25 mL) was added rapidly. The dark reaction mixture was stirred for 4 h without external cooling. The mixture of heavy oil and water was decanted from some dark brown gum and extracted with Et₂O. Evaporation of the dried (Na₂SO₄) organic layer gave 22.1 g (98%) of dark oil that was distilled in vacuo. Fractions containing material of sufficient purity for use as an intermediate totaled 14.9 g (66%).

Synthesis of 2-Amino-1,5-dihydro-7-substituted-4H-pyrrolo[3,2-d]pyrimidin-4-ones (11) from Compounds 3 (Scheme I). Standard Procedure: Synthesis of compounds 2-amino-1,5-dihydro-7-[(4-hydroxyphenyl)methyl]-4H-pyrrolo[3,2-d]pyrimidin-4-one (11g), its debenzylated product 11j, and 2-amino-7-[(3-chlorophenyl)methyl]-1,5-dihydro-4H-pyrrolo[3,2-d]pyrimidin-4-one (11l) are described to illustrate standard procedures by which the compounds in Table IX were prepared.
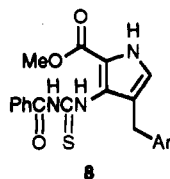
Table VI

7

no.	Ar	% yield[a]	mp, °C	PM[b]	MS, m/z	NH	NH2	H-5	$J_{H-5,NH}$ (Hz)
						1H-NMR chemical shifts, δ			
a	2-C4H3O	87.4[c]	133-134	A	220 (M)+ (EI)	10.51	4.85	6.52	3.3
b	2-C4HS	60.9	111-112	A	237 (M + H)+ (FAB)	10.50	4.85	6.55	d
c	3-C4H3S	68	108-109	B	237 (M + H)+ (FAB)	10.46	4.85	6.49	3.4
d	C6H5	88	96-98	C					
e	2-BzlOC6H4	76[e]	–	C					
f	3-BzlOC6H4	69	107-108	D	336 (M)+ (EI)	10.49	4.82	6.50	3.2
g	4-BzlOC6H4	82[c]	159-160	A	336 (M)+ (FAB)	10.45	4.80	6.43	3.4
k	2-ClC6H4	86.2	115-116	D	264 (M)+ (EI)	10.55	4.90	6.41	d
p	4-IC6H4	89.4[c]	–	E					
q	3-FC6H4	–	101-102	B	248 (M)+ (FAB)	10.53	4.90	6.56	3.4
r	3-MeC6H4	68.6	88-89	F	244 (M)+ (EI)	10.46	4.83	6.46	3.2
s	3-MeOC6H4	62.7	58-60	E	260 (M)+ (EI)	10.47	4.85	6.50	3.5
t	3-CF3C6H4	66.8	110	F	298 (M)+ (EI)	10.55	4.95	6.65	3.4
u	3,4-Cl2C6H3	76.8	115	D	299 (M)+ (EI)	10.56	4.92	6.56	d
v	2,3,5-Cl3C6H2	77	142	D	333 (M + H)+ (FAB)	10.66	4.98	6.57	3.2
w	3-C5H4N	59	135-136	G					

[a] Represents overall yields from enaminonitriles 4. [b] Purification method: A, crystallized from toluene/cyclohexane (1:4); B, column chromatography on silica gel (CHCl3 eluent) and recrystallized from toluene/cyclohexane (1:3); C, column chromatography on silica gel using CHCl3/MeOH (98:2) as the eluent; D, crystallized from methanol; E, washed with ether and used in the next step without further purification; F, flash column chromatography using CHCl3/methanol (97:3) as the eluent and recrystallized from CHCl3/ether (5:95); G, crystallized from toluene. [c] Represents crude yield. [d] Unresolved.

Table VII

8

no.	Ar	% yield	mp, °C	PM[a]
a	2-C4H3O	96.8	153-154	A
b	2-C4H3S	95.5	166-167	A
c	3-C4H3S[b]	92	–	–
d	C6H5	95	145	B
e	2-BzlOC6H4	89	204-205	C
f	3-BzlOC6H4	91.6	133-134	D
g	4-BzlOC6H4	97	114-115	E
k	2-ClC6H4	98	174-175	F
p	4-IC6H4	76	153-154	G
q	3-FC6H4	97	164-165	A
r	3-MeC6H4	87	151-152	F
s	3-MeOC6H4	85	153-154	D
t	3-CF3C6H4	86.5	163-164	B
u	3,4-Cl2C6H3	93	185-186	B
v	2,3,5-Cl3C6H2	90.8	179-180	B
w	3-C5H4N	99	155-157	H

[a] After completion of the reaction, solvent was evaporated and the resulting solid was purified by using the following procedures: A, washed with ether to give a solid of sufficient purity to use in the next step; B, washed with methanol and recrystallized from CHCl3/ether (1:9); C, purified by column chromatography on silica gel using CHCl3 as the eluent and then recrystallized from ether/hexane (3:1); D, washed first with methanol and then with ether; E, crystallized from toluene/cyclohexane; F, washed with methanol; G, purified by silica gel column chromatography (CHCl3) and recrystallized from toluene/cyclohexane (1:3); H, washed with cyclohexane ether. [b] Used in the next step without purification.
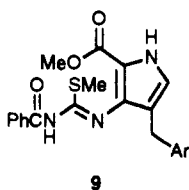
2-Formyl-3-[4-(benzyloxy)phenyl]propanenitrile (3g). Under a nitrogen atmosphere, ethyl formate (7.38 g, 99.6 mmol) in anhydrous THF (100 mL) was added dropwise (rapidly) to a stirred mixture of NaH (1.75 g, 72.9 mmol) and 2g (8.89 g, 37.5 mmol) in THF (100 mL). Steady H2 evolution was observed over a 5-h period (mineral oil bubbler), and the reaction was

allowed to continue overnight, becoming a dark amber color. Additional portions of NaH and HCO2Et (2 equiv each) were added, and the mixture was refluxed for 30 min (necessary only for 3e and 3g) and then stirred at room temperature overnight. Solvent was evaporated, and a slurry of the residual gum in ice-cold water (100 mL) was adjusted to pH 6 with cold 6 N HCl and extracted with CHCl3 (3 × 100 mL). The extract was washed with H2O (100 mL), dried (Na2SO4), and evaporated. The semisolid residue was triturated with hexane, which was decanted. Column chromatography of the residue on silica gel (using CHCl3 as eluent) gave 6.45 g (73%) of recovered nitrile starting material. Continued elution with CHCl3/MeOH (98:2) gave 1.48 g (17%) of the desired formyl compound 3g, MS (EI) 265 (M)+, 197 (265 – CH(CN)CHO)+, 107 (PhCH2O)+, 91 (PhCH2)+.

2-[4-(Benzyloxy)benzyl]-3-[(2-methoxy-2-oxoethyl)amino]-2-propenenitrile (4g). A solution of the formyl compound 3g (1.41 g, 5.31 mmol), methyl glycinate hydrochloride (1.00 g, 7.97 mmol), and sodium acetate (0.654 g, 7.97 mmol) in MeOH (40 mL) and H2O (10 mL) was stirred at room temperature for 48 h. The residual mixture of water and dark oil was extracted with CHCl3 (2 × 25 mL), and the organic extract was washed with H2O (20 mL), dried (Na2SO4), and evaporated to give 4g as a viscous orange gum: yield 1.52 g (85%); MS (EI) 336 (M)+, 277 (336 – CO2CH3)+, 263 (336 – CH2CO2CH3)+, 245 (336 – CH2Ph)+. In the NMR spectrum some of the resonance peaks occurred in pairs because the product was a 1:1 mixture of cis–trans isomers: 1H-NMR (CDCl3) δ 3.31, 3.37 (2 s, 2 each, CH2C=C), 3.75, 3.77 (2 s, 3 each, CO2CH3), 3.82, 3.92 (2 d, 2 each, NHCH2CO2CH3), 4.54, 4.86 (2 m, 1 each, NHCH2CO2CH3), 5.04 (s, 2, OCH2C6H5), 6.39, 6.64 (2 d, 1 each, C=CHNH), 6.92, 7.15, 7.38 (complex multiplets, aromatic CH).

2-[4-(Benzyloxy)benzyl]-3-[(ethoxycarbonyl)(2-methoxy-2-oxoethyl)amino]-2-propenenitrile (5g) and 1-Ethyl 2-Methyl 3-Amino-4-[4-(benzyloxy)benzyl]-1H-pyrrole-1,2-dicarboxylate (6g). A solution of the enamine 4g (1.5 g, 4.5 mmol) in dry CH2Cl2 (25 mL) was cooled to 0 °C and treated with 1,5-diazabicyclo[4.3.0]non-5-ene (DBN, 1.12 g, 9.04 mmol) followed by ethyl chloroformate (0.735 g, 6.78 mmol). After refrigeration for 24 h, 0.2 mL of DBN and 0.1 mL of ClCO2Et were added to consume the small quantity of remaining starting material, then an additional equivalent of DBN (0.6 g) was added, and the mixture was refrigerated for 20 h. Although TLC showed a small quantity of uncyclized intermediate 5g was still present,

Table VIII

9

no.	Ar	% yield	mp, °C	PM^a	MS, m/z	^{1}H-NMR chemical shifts, δ NH	NH$_2$	H-5	$J_{H-5,NH}$ (Hz)
a	2-C$_4$H$_3$O	99^b	c	A	398 (M + H)$^+$ (FAB)	12.06	2.49	6.87	3.2
b	2-C$_4$H$_3$S	72	116–117	B	414 (M + H)$^+$ (FAB)	12.06	2.50	6.89	3.0
c	3-C$_4$H$_3$S	83	c	A	414 (M + H)$^+$ (FAB)	12.03	2.50	6.82	2.8
d	C$_6$H$_5$	98^b	c	C					
e	2-BzlOC$_6$H$_4$	84^b	c	A					
f	3-BzlOC$_6$H$_4$	97	c	A					
g	4-BzlOC$_6$H$_4$	99^b	c	A		11.98	2.47	6.76	2.9
k	2-ClC$_6$H$_4$	93.8	c	D	441 (M)$^+$ (EI)	12.05	2.47	6.77	3.0
p	4-IC$_6$H$_4$	81.3	c	D	534 (M + H)$^+$ (FAB)	12.03	2.45	6.83	d
q	3-FC$_6$H$_4$	83	c	A					
r	3-MeC$_6$H$_4$	95	129–130	D	421 (M)$^+$ (EI)	12.0	2.47	6.81	3.0
s	3-MeOC$_6$H$_4$	93^b	c	C					
t	3-CF$_3$C$_6$H$_4$	97.5^b	c	C					
u	3,4-Cl$_2$C$_6$H$_3$	99^b	c	C					
v	2,3,5-Cl$_3$C$_6$H$_2$	91.6	164–165	E	510 (M + H)$^+$ (FAB)	12.08	2.42	6.95	d
w	3-C$_5$H$_4$N	88	189–190	D					

^{a} Purified by using the following methods: A, column chromatography on silica gel using CHCl$_3$ as the eluent; B, column chromatography on silica gel (CHCl$_3$ eluent) and recrystallized from cyclohexane; C, used in the next step without further purification; D, column chromatography on silica gel using CHCl$_3$/methanol (98:2) as the eluent; E, crystallized from methanol and recrystallized from CHCl$_3$/ether (5:95). ^{b} Crude yield. ^{c} Foam. ^{d} Unresolved.

along with a major quantity of 6g, solvent was evaporated and the gummy residue was chromatographed on a silica gel column (CHCl$_3$ eluent) in order to obtain a sample of 5g for spectral purposes. The 30-mg fraction believed to be 5g was submitted to infrared and mass spectral analysis. MS (EI) 408 (M)$^+$, IR 2210 cm^{-1} (CN). The pyrrole 6g has the same molecular ion but the CN band in the infrared is absent. The 30-mg sample and those column fractions containing 5g were dissolved in CH$_2$Cl$_2$ (15 mL) containing 0.5 mL of DBN and refrigerated overnight to complete cyclization to 6g. Column chromatographic purification (CHCl$_3$ as the eluent) gave 1.40 g (76%) of 6g.

Methyl 3-Amino-4-[4-(benzyloxy)benzyl]-1H-pyrrole-2-carboxylate (7g). Anhydrous Na$_2$CO$_3$ (361 mg, 3.41 mmol) was added to a solution of the N-blocked pyrrole 6g (1.39 g, 3.40 mmol) in MeOH (25 mL), and the mixture was stirred at room temperature for 24 h with some product separation observed after ~15 min. Solvent was evaporated, and a solution of the organic residue in CHCl$_3$ was filtered to remove inorganics, washed by shaking with H$_2$O, dried (Na$_2$SO$_4$), and evaporated to give 7g as a yellow solid residue, yield 1.10 g (96%). Recrystallization from toluene/cyclohexane 1:1 (30 mL) gave an analytical sample of 7g as pale yellow crystals (0.939 g, 82%): mp 159–160 °C; MS (EI) 336 (M)$^+$, 304 (336 − CH$_3$OH)$^+$, 276 (336 − CH$_3$CO$_2$H)$^+$, 245 (336 − CH$_2$Ph)$^+$, (336 − OCH$_2$Ph + H)$^+$; UV (0.1 N HCl) λ 225 (16.8), 270 (18.2), (pH 7 buffer) 270 (20.0), (0.1 N NaOH) 271 (20.1). ^{1}H-NMR (DMSO-d_6) δ 3.55 (s, 2, PhCH$_2$-pyrrole), 3.68 (s, 3, CH$_3$CO$_2$), 4.80 (br s, 2, NH$_2$), 5.04 (s, 2, PHCH$_2$O), 6.44 (d, 1, pyrrole ring proton), 6.89, 7.12, 7.37 (d, d, complex multiplet; 2, 2, 5; aromatic CH), 10.44 (br s, 1, pyrrole NH). Anal. (C$_{20}$H$_{20}$N$_2$O$_3$) C, H, N.

Methyl 3-[[(Benzoylamino)thioxomethyl]amino]-4-[4-(benzyloxy)benzyl]-1H-pyrrole-2-carboxylate (8g). Under a nitrogen atmosphere, a solution of the pyrrole (7g, 906 mg, 2.69 mmol) and benzoyl isothiocyanate (527 mg, 3.20 mmol) in dry CH$_2$Cl$_2$ (50 mL) was stirred at room temperature for 1 h. The solvent was evaporated, and the residue was washed first with hexane and then with hexane/Et$_2$O (1:1) by trituration and decantation, yield 1.33 g (97%). A portion (105 mg) of this material was recrystallized from cyclohexane to give 8g as a white crystalline solid that was dried in vacuo over P$_2$O$_5$ at 65 °C: yield 78 mg; mp 114–115 °C; MS (FAB) 500 (M + H)$^+$; UV (pH 1 and pH 7) compound precipitates from EtOH solution, (pH 13) unstable, maximum at 279 nm. ^{1}H-NMR (DMSO-d_6) δ 3.72
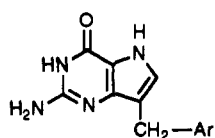
(apparent s, 5, CO$_2$CH$_3$ superimposed on C$_6$H$_4$CH$_2$), 4.94 (s, 2, C$_6$H$_5$CH$_2$O), 6.69 (d, 1, pyrrole H-5), 6.84, 7.08 (2 d, 2 each, aromatic CH of C$_6$H$_4$CH$_2$), 7.33 (complex m, 5, aromatic CH of C$_6$H$_5$CH$_2$O), 7.54 (t, 2, aromatic CH of C$_6$H$_5$CO), 7.66 (t, 1, p-CH of C$_6$H$_5$CO), 7.97 (d, 2, OCH's of C$_6$H$_5$CO), 11.59, 12.06 [2 s, 1 each, NHC(O) and NHC(S)], 11.82 (br s, 1, pyrrole NH). Anal. (C$_{28}$H$_{25}$N$_3$O$_4$S) C, H, N.

Methyl 3-[[[(Benzoylamino)methylthio]methylene]amino]-4-[4-(benzyloxy)benzyl]-1H-pyrrole-2-carboxylate (9g). A solution of 8g (1.207 g, 2.42 mmol) and DBN (0.360 g, 2.90 mmol) in dry CH$_2$Cl$_2$ (40 mL) was cooled to 0 °C and treated with methyl iodide (0.754 g, 5.32 mmol). The solution was stirred at 0 °C for 15 min and then at room temperature for 1 h. The solvent was evaporated, and the gummy residue was chromatographed on a short silica gel column (CHCl$_3$ eluent) to give 1.25 g (100%) of the methylthio compound 9g. This material was used directly in the next step: ^{1}H-NMR (DMSO-d_6) δ 2.46 (s, 3, SCH$_3$), 3.63 (s, 2, C$_6$H$_4$CH$_2$), 3.69 (s, 3, CO$_2$CH$_3$), 5.00 (s, 2, C$_6$H$_5$CH$_2$O), 6.75 (d, 1, pyrrole H-5), 6.85, 7.08 (2 d, 2 each, aromatic CH of C$_6$H$_4$), 7.37 (complex m, 5, aromatic CH of C$_6$H$_5$CH$_2$O), 7.48 (t, 2, aromatic CH of C$_6$H$_5$CO), 7.57 (t, 1, p-CH of C$_6$H$_5$CO), 8.18 (d, 2, OCH's of C$_6$H$_5$CO), 11.5 very broad, best seen in the integral, 1, NHCO), 11.97 (br s, 1, pyrrole NH).

2-Amino-7-[4-(benzyloxy)benzyl]-1,5-dihydro-4H-pyrrolo[3,2-d]pyrimidin-4-one (11g) and 7-[4-(Benzyloxy)benzyl]-1,5-dihydro-2-(methylthio)-4H-pyrrolo[3,2-d]pyrimidin-4-one (10g). A solution of 9g (1.2 g, 2.33 mmol) in MeOH (150 mL) saturated with NH$_3$ at 0 °C was heated at 90–95 °C for 24 h in a glass-lined stainless steel bomb and then allowed to cool to room temperature and stand overnight, depositing white crystals that were collected by filtration, yield 377 mg (47%). The product was extracted continuously into MeOH in a Soxhlet apparatus. The deposit of white crystalline solid was collected and dried in vacuo over P$_2$O$_5$ at 65 °C for 4 h; yield of 11g was 335 mg (41%). See Table IX for data on 11g.

Column chromatography of the filtrate from the above procedure on silica gel (CHCl$_3$/MeOH 95:5 with 10 mL of HOAc per liter) gave three main products besides benzamide: an additional 120 mg (15%) of the desired product 11g, 170 mg (19%) of the 2-(methylthio) byproduct 10g, and 180 mg of a previously unseen product tentatively assigned as the 9-deaza-xanthine analog on mass spectral evidence (MS (FAB) 348 (M + H)$^+$). Recrystallization of a portion of 10g from MeOH/H$_2$O

Table IX

11

no.	Ar	mp, °C	analytical/spectral data
a	2-C₄H₃O	244–245	MS (FAB): 231 (M + H)⁺. UV: 0.1 N HCl 230 (19.7), 273 (15.4); pH 7 228 (27.6), 271 (11.5); 0.1 N NaOH 263 (8.8), 285 (8.10). Anal. (C₁₁H₁₀N₄O·0.1C₅H₁₀O₂ (isopropyl acetate)) C, H, N.
b	2-C₄H₃S	268–269	MS (EI): 246 (M⁺), 228 (246 – H₂O)⁺, 213 (246 – SH)⁺, 163 (246 – C₄H₃S)⁺. Anal. (C₁₁H₁₀N₄OS·0.25C₅H₁₀O₂ (isopropyl acetate)) C, H, N.
c	3-C₄H₃S	270–271	MS (FAB): 246 (M + H)⁺; UV: 0.1 N HCl 235 (22.5), 274 (15.8); pH 7 233 (25.6), 272 (10.8); 0.1 N NaOH 230 (25.8), 265 (7.8), 286 (6.8). Anal. (C₁₁H₁₀N₄OS) C, H, N.
d	C₆H₅	269–270	MS (EI): 240 (M⁺), 163 (240 – C₆H₅)⁺. UV: 0.1 N HCl 235 (16.9), 274 (15.0); pH 7 233 (21.0), 272 (10.3); 0.1 N NaOH 264 (7.5), 287 (6.5). Anal. (C₁₃H₁₂N₄O) C, H, N.
f	3-BzlOC₆H₄	228–230	MS (FAB): 347 (M + H)⁺. UV: 0.1 N HCl 232 (17.3), 275 (15.4); pH 7 272 (11.2); 0.1 N NaOH 268 (8.2). Anal. (C₂₀H₁₈N₄O₂) C, H, N.
g	4-BzlOC₆H₄	250–251	MS (FAB): 347 (M + H)⁺, 255 (346 – CH₂Ph)⁺, 163 (346 – PhOCH₂Ph)⁺. UV: 0.1 N HCl 229 (26.0), 274 (16.9); pH 7 unstable, precipitates; 0.1 N NaOH 227 (32.7), 267 (8.8). Anal. (C₂₀H₁₈N₄O₂) C, H, N.
h	2-HOC₆H₄	260–261	MS (FAB): 257 (M + H)⁺. UV: Precipitates at all 3 pH's; 0.1 N HCl 234, 275; pH 7 231, 272; 0.1 N NaOH 232, 266 (sh) 290. Anal. (C₁₃H₁₂N₄O₂·0.1C₂H₆O (EtOH)) C, H, N.
i	3-HOC₆H₄	278–280	MS (FAB): 257 (M + H)⁺. UV: 0.1 N HCl 274 (17.7); pH 7 273 (12.5); 0.1 N NaOH 270 (8.8), 289 (10.2). Anal. (C₁₃H₁₂N₄O₂·0.4MeOH) C, H, N.
j	4-HOC₆H₄	>350	MS (EI): 256 (M⁺), 238 (256 – H₂O)⁺, 162 (256 – PhOH)⁺. UV: 0.1 N HCl 230 (21.0), 274 (17.0); pH 7 229 (25.7), 273 (12.3); 0.1 N NaOH 234 (30.5), 266 (sh), 290 (9.2). Anal. (C₁₃H₁₂N₄O₂·0.12EtOH) C, H, N.
k	2-ClC₆H₄	279–280	MS (EI): 274 (M)⁺, 239 (274 – Cl)⁺. UV: 0.1 N HCl 234 (19.1), 274 (16.4); pH 7 231 (23.8); 272 (10.8); 0.1 N NaOH 265 (7.9), 287 (6.7). Anal. Calcd for C₁₃H₁₁ClN₄O·0.3(C₂H₅)₂O·0.04CHCl₃: C, 56.69; H, 4.69; N, 18.57. Found: C, 56.99; H, 4.32; N, 19.01.
l	3-ClC₆H₄	258	MS (EI): 274 (M)⁺, 239 (274 – Cl)⁺. UV: 0.1 N HCl 274 (15.2); pH 7 271 (10.4); 0.1 N NaOH 266 (7.7), 288 (6.6). Anal. (C₁₃H₁₁ClN₄O·0.25H₂O) C, H, N.
m	4-ClC₆H₄	207–208	MS (FAB): 257 (M + H)⁺. UV: 0.1 N HCl 274 (17.0); pH 7 272 (11.5); 0.1 N NaOH 265 (8.4). Anal. (C₁₃H₁₁ClN₄O) C, H, N.
p	4-IC₆H₄	320–322	MS (FAB): 367 (M + H)⁺. UV: 0.1 N HCl 235 (32.4), 274 (17.2); pH 7 234 (36.2), 272 (11.8); 0.1 N NaOH 232 (36.8), 266 (sh), 290 (sh). Anal. (C₁₃H₁₁IN₄O·0.2HOAc·0.5H₂O) C, H, N.
q	3-FC₆H₄	297–298	MS (FAB): 259 (M⁺), (PhOH)⁺. UV: 0.1 N HCl 235 (32.4), 273 (15.7); pH 7 233 (22.0), 270 (10.8); 0.1 N NaOH 228 (22.4), 263 (8.1), 268 (7.9), 287 (6.6). Anal. (C₁₃H₁₁FN₄O) C, H, N.
r	3-MeC₆H₄	253	MS (FAB): 255 (M + H)⁺. UV: 0.1 N HCl 234 (17.8), 274 (15.7); pH 7 231 (21.8), 273 (11.1); 0.1 N NaOH 266 (7.7). Anal. (C₁₄H₁₄N₄O·H₂O) C, H, N.
s	3-MeOC₆H₄	235	MS (FAB): 271 (M + H)⁺. UV: 0.1 N HCl 231 (18.9), 274 (16.9); pH 7 272 (12.0); 0.1 N NaOH 270 (8.7). Anal. (C₁₄H₁₄N₄O₂·H₂O) C, H, N.
t	3-CF₃C₆H₄	239–240	MS (FAB): 309 (M + H)⁺. UV: 0.1 N HCl 235 (17.4); 273 (15.7); pH 7 234 (21.5); 272 (10.7); 0.1 N NaOH 265 (8.2); 287 (6.7). Anal. Calcd for C₁₄H₁₁F₃N₄O: C, 54.54; H, 3.59; N, 18.17. Found: C, 54.20; H, 4.08; N, 18.02.
u	3,4-Cl₂C₆H₃	278–280	MS (FAB): 309 (M + H)⁺. UV: 0.1 N HCl 274 (16.0); pH 7 273 (10.6); 0.1 N NaOH 264 (7.9); 283 (7.2). Anal. (C₁₃H₁₀N₄OCl₂) C, H, N.
v	2,3,5-Cl₃C₆H₂	>300	MS (FAB): 343 (M + H)⁺. UV: 0.1 N HCl 232 (24.8); 274 (15.1); pH 7 271 (9.7); 0.1 N NaOH 286 (6.6). Anal. (C₁₃H₉N₄OCl₃) C, H, N.
w	3-C₅H₄N	>315	MS (FAB): 242 (M + H)⁺. UV: 0.1 N HCl 233 (18.2), 269 (17.4); pH 7 233 (18.2), 269 (17.4); pH 7 233 (22.4); 269 (12.3); 0.1 N NaOH 227 (22.2), 263 (10.5), 290 (sh). Anal. (C₁₂H₁₁N₅O) C, H, N.

(2:1, 15 mL) gave crystalline material: mp 179–181 °C; MS (FAB) 378 (M + H)⁺; ¹H-NMR (DMSO-d_6) δ 2.52 (s, 3, SCH₃), 3.82 (s, 2, C₆H₄CH₂), 5.04 (s, 2, PhCH₂O), 6.88, 7.22 (d, d, 2 each, aromatic CH of CH₂C₆H₄OCH₂), 7.10 (d, 1, pyrrole ring proton), 7.36 (complex multiplet, 5, aromatic CH of OCH₂C₆H₅), 11.70 (d, 1, pyrrole NH), 12.05 (s, 1, NHC(O)).

2-Amino-1,5-dihydro-7-(4-hydroxybenzyl)-4H-pyrrolo-[3,2-d]pyrimidin-4-one (11j). A suspension of 11g (338 mg, 0.976 mmol) in EtOH (275 mL) was hydrogenated at room temperature and atmospheric pressure. Consumption of H₂ was very slow, so the reaction mixture was heated in a large water bath (55 °C), which was allowed to cool slowly to room temperature. Hydrogenolysis of the benzyl protective group was complete in about 5 h (TLC). The reaction mixture was warmed to dissolve precipitated product and filtered through a thin Celite pad under N₂ pressure. The solid obtained by evaporation of the solvent was recrystallized from the minimum volume of EtOH to give 11j as white crystals that were dried in vacuo over P₂O₅ at 65 °C: yield 156 mg (62%), mp chars, but does not melt below 350 °C. An additional 52 mg (21%) of product was obtained by concentration of the filtrate.

3-(3-Chlorophenyl)-2-formylpropanenitrile (31). Sodium hydride (2.43 g, 101 mmol, 1.4 equiv) was suspended in dry THF

(80 mL) under an atmosphere of dry N₂ and to this was added ethyl formate (24.69 g, 330 mmol, 4.6 equiv) and 2-(chlorophenyl)-propanenitrile (2c, 12.0 g, 72.46 mmol) under stirring. The reaction mixture was stirred at room temperature for 24 h. Volatile matter was evaporated in vacuo at room temperature. Water (50 mL) was added to the residue at 0 °C, and the solution was acidified to pH 5 by 10% HCl with ice bath cooling. The precipitate of heavy oil was extracted with ethyl acetate (100 mL), washed with water (2 × 40 mL), and dried (Na₂SO₄). The organic layer was evaporated to give a red-brown oil (14.20 g) which was used in the next step without further purification.

2-(3-Chlorobenzyl)-3-[(2-methoxy-2-oxoethyl)amino]-2-propenenitrile (41). Methyl glycinate hydrochloride (13.46 g, 108.6 mmol, 1.5 equiv) and sodium acetate (8.9 g, 108.6 mmol, 1.5 equiv) were added to a solution of crude 31 (14.20 g) in a mixture of methanol (137 mL) and H₂O (34 mL), and the resulting solution was stirred at room temperature for 24 h. After evaporation of methanol at room temperature, the residual mass was extracted with ethyl acetate. The organic layer was washed with H₂O (2 × 40 mL), dried (Na₂SO₄), and evaporated to give an amber oil which was purified by flash column chromatography over silica gel using chloroform as the eluent to give 41 (oil) as a mixture of cis–trans isomers (10.86 g, 56.7%, overall yield from

21): MS (EI) m/z 264 (M)$^+$, 229 (264 – Cl)$^+$, 205 (264 – CO_2CH_3)$^+$; IR (capillary film), 3350 (NH), 2191 (CN), 1748 (CO_2Me), 1646 (C=C); ^{1}H-NMR (DMSO-d_6) δ 3.32 (s, 0.8, CH_2), 3.40 (s, 1.2, CH_2), 366 (s, 1.2, OCH_3), 3.68 (s, 1.8, OCH_3), 3.93 (d, 0.8, CH_2N), 3.97 (d, 1.2, CH_2N), 6.75, 6.81 (two overlapping t, 1, NH's), 6.89–6.99 (m, 1, aromatic H), 7.12–7.38 (m, 4, three aromatic H and HC=C). Anal. ($C_{13}H_{13}N_2O_2Cl$) C, H, N.

1-Ethyl 2-Methyl 3-Amino-4-(3-chlorobenzyl)-1*H*-pyrrole-1,2-dicarboxylate (61). To an ice-cooled solution of enamine 41 (7.35 g, 27.8 mmol) in dry dichloromethane (80 mL) was added DBN (10.35 g, 83.3 mmol, 3 equiv) and ethyl chloroformate (4.52 g, 41.65 mmol, 1.5 equiv) under nitrogen. The solution was stirred for 24 h at room temperature. Volatile matter was evaporated in vacuo to give a thick gummy residue that was purified by flash column chromatography over silica gel using $CHCl_3$ as the eluent to give crude 61 as an oil (8.19 g, 87.6%) that was used in the next step without further purification.

Methyl 3-Amino-4-(3-chlorobenzyl)-1*H*-pyrrole-2-carboxylate (71). To a solution of crude 61 (8.19 g, 24.3 mmol) in MeOH (130 mL) was added Na_2CO_3 (6.44 g, 60.84 mmol, 2.5 equiv). The reaction mixture was stirred at room temperature for 24 h. Solid sodium carbonate was removed by filtration and washed well with MeOH. The methanol solution was reduced to a volume of ~15 mL and kept in the refrigerator for 2 h to give 2.8 g of crystalline product. Further concentration of the mother liquor gave an additional 3.22 g of pure 71: total yield 6.02 g (82%); mp 105–106 °C; MS (FAB) m/z 264 (M)$^+$, 233 (264 – OCH_3)$^+$; IR (KBr) 3393, 3305, 3142, 3062.7, 2927, 1678, 1596, 1517; ^{1}H-NMR (DMSO-d_6) δ 3.65 (s, 2, CH_2), 3.69 (s, 3, CO_2CH_3), 4.9 (bs, 2, D_2O exchangeable, NH_2), 6.57 (d, 1, pyrrole ring proton), 7.24 (m, 4 H, aromatic CH), 10.56 (bs, 1, pyrrole NH). Anal. ($C_{13}H_{13}N_2O_2$-Cl) C, H, N.

Methyl 3-[[(Benzoylamino)thioxomethyl]amino]-4-(3-chlorobenzyl)-1*H*-pyrrole-2-carboxylate (81). To a solution of 71 (1.0 g, 3.78 mmol) in dry dichloromethane (20 mL) was added benzoyl isothiocyanate (0.69 g, 4.26 mmol) under N_2 at room temperature. The reaction mixture was stirred for 1 h and evaporated to dryness, and the light yellow residue was triturated with methanol. The white crystalline material was isolated by filtration and recrystallized from $CHCl_3$/ether mixture to give the required thioureido compound 81 as an analytical pure sample (1.3 g, 81.2%): mp 160–161 °C; MS (EI) m/z 427 (M)$^+$, 368 (427 – CO_2CH_3)$^+$, 306 (427 – NH_2 – C(O) – Ph)$^+$; IR (KBr) 3266 (pyrrole NH), 1688, 1675 (C(O)–NH); ^{1}H-NMR (DMSO-d_6) δ 3.72 (s, 3, CO_2CH_3), 3.82 (s, 2-CH_2), 6.81 (d, 1, pyrrole CH), 7.19 (m, 4, m-chlorophenyl CH), 7.53, 7.66, and 7.96 (t, t, d, 2, 1, 2, benzoyl CH), 11.62, 12.07 (2 s, 1 each, NHC(S)NH), 11.89 (d, 1, pyrrole NH). Anal. ($C_{21}H_{18}N_3O_3ClS$) C, H, N.

Methyl 3-[[[(Benzoylamino)methylthio]methylene]amino]-4-(3-chlorobenzyl)-1*H*-pyrrole-2-carboxylate (91). To an ice-cooled solution of 81 (0.71 g, 1.66 mmol) in dry CH_2Cl_2 (50 mL) was added DBN (0.24 g, 1.9 mmol) and methyl iodide (0.68 g, 4.8 mmol). The reaction mixture was stirred at 0 °C for 1 h. Solvent was evaporated and the residue was extracted with $CHCl_3$, washed with H_2O (2 × 30 mL), dried (Na_2SO_4), and evaporated to give a glassy thick oil that was purified by flash column chromatography over silica gel using $CHCl_3$ as the eluent to yield 91 as a glassy foam (0.67 g, 92%). A small amount of sample was crystallized from MeOH: mp 121 °C; MS (EI) m/z 441 (M)$^+$, 426 (441 – CH_3)$^+$, 394 (441 – SCH_3)$^+$; IR (KBr) 3306 (pyrrole NH), 1684 [C(O)OMe]; ^{1}H-NMR (DMSO-d_6) δ 2.46 (s, 3, SCH_3), 3.72 (s, 3, CO_2CH_3), 3.74 (s, 2, CH_2), 6.88 (d, 1, J = 3 Hz, pyrrole CH), 7.18 (m, 4, chlorophenyl CH), 7.48, 7.56 (2 m, 2 each, benzoyl CH), 8.17 (bs, 2, benzoyl CH), PhCONH (very broad, seen in the integral 11.4–11.9), 12.03 (bs, 1, pyrrole NH).

2-Amino-7-(3-chlorobenzyl)-1,5-dihydro-4*H*-pyrrolo[3,2-*d*]pyrimidin-4-one (111). A solution of the methylthio intermediate 91 (0.6 g, 1.35 mmol) in MeOH saturated with ammonia (40 mL) was heated at 110 °C for 20 h in a glass-lined steel bomb. The reaction mixture was cooled to room temperature and then evaporated to dryness. Purification of the crude mixture by flash column chromatography over silica gel using $CHCl_3$ as eluent removed 101 then $CHCl_3$/MeOH (95:5) gave pure 111 (190 mg, 51%). See Table IX for data on 111.

Biologic Evaluations. In Vitro Enzyme Inhibition Studies. Assays of candidate compounds were performed by incu-

bating the inhibitors at various concentrations with 10 μM [8-^{14}C]inosine and 0.001 units of calf spleen PNP (Sigma Chemical Co.) in 50 mM phosphate buffer, pH 7.4 (total volume 0.5 mL) for 10 min. Assays were also performed at 1 mM phosphate concentration in 100 mM HEPES buffer, pH 7.4. Hypoxanthine and inosine were separated by paper chromatography and the ^{14}C present in the hypoxanthine spots was determined by liquid scintillation spectrometry. Each series of experiments contained a control that was assayed at multiple times to assure that the enzyme reaction proceeded normally and a known inhibitor, ATG or 8-aminoguanosine. The IC_{50} values were calculated from plots of % inhibition vs drug concentration (Table I). K_i values were determined from Lineweaver–Burk plots using the coupled xanthine oxidase assay.[66] Values obtained are shown in Table III. Assays of 8-amino/desamino pairs were carried out using PNP isolated from human erythrocytes to compare with literature values for guanine/8-aminoguanine pairs (Table II).

X-ray Crystallographic Analysis. Crystals of PNP used for X-ray diffraction studies were prepared from ammonium sulfate solutions using vapor diffusion techniques as previously described.[38] The crystals were grown from 4-μL drops hanging from siliconized microscope cover slips over the wells of a Linbro cell culture plate. The droplet consisted of 2 μL of 10–20 mg/mL of protein solution in 10 mM potassium phosphate buffer (pH = 7.1) plus 2 μL of 35–40% saturated ammonium sulfate solution in 50 mM citrate buffer (pH = 5.3). The droplet was equilibrated at room temperature against 1 mL of 35–40% saturated ammonium sulfate solution in 50 mM citrate buffer at pH 5.3 that was contained in the well of the Linbro plate. Rhombohedral-shaped crystals with dimensions up to 0.5 mm formed after 3–5 days. For X-ray studies these crystals were transferred to 55% saturated ammonium sulfate solution in 50 mM citrate buffer at pH 5.4 and stored at room temperature for up to several months.

Complexes between PNP and inhibitor molecules were prepared by transferring a preformed PNP crystal into 2 mL of the ammonium sulfate stabilizing solution described above in which the inhibitor has been dissolved. The final concentration of inhibitor was 1 mM or sometimes less for compounds with poor solubility. For these compounds, saturating amounts were added to the solution plus a small amount of excess solid. The PNP crystal was allowed to equilibrate for 24 h and then removed from the solution and mounted in a sealed glass capillary for X-ray intensity measurements.

All X-ray intensity measurements were recorded with a Nicolet/Siemens X-100 multiwire area detector. The X-rays were produced by a Rigaku RU-300 rotating anode generator operating at 100 mA and 50 kV with a 0.3 × 3 mm focus and a Cu anode. The X-ray beam was reflected from a graphite monochromator and passed through a 0.25-mm collimator. The crystal to detector distance was 160 mm and the detector was offset by 15° relative to the direct X-ray beam. X-ray intensity data was measured on 0.25° oscillation frames at 300 s of exposure per frame. Each crystal yielded from 300–500 frames of data before radiation damage prevented further measurements. One to three crystals were used for each PNP/inhibitor complex depending on crystal size and data quality.

The X-ray intensity data were reduced using the XENGEN package of programs. The integrated intensities were then scaled and merged to produce a final data set containing only unique reflections (Table X). The R-value for different measurements of equivalent reflections ranged from 8–12%. The final data sets were reasonably complete at 3.0-Å resolution with some data present between 3.0- and 2.8-Å resolution. The percent of possible reflections observed from a single crystal ranged from about 50–90% at 3.0 Å resolution depending on the initial orientation of the crystallographic three-fold axis and the number of data frames that were measured. For difference Fourier calculations the data for the PNP complexes was scaled to the native data using relative Wilson plots. The fractional change in intensity relative to the native data set ranged from 14–20%.

Difference Fourier maps were calculated at 3.2-Å resolution using F(complex) – F(native) as the Fourier coefficient and calculated phases from 5–3.2-Å resolution and experimentally determined phases from 10–5-Å resolution. Analysis of the difference electron density was performed on an Evans and

Table X. Summary of X-ray Crystallographic Data for PNP/Inhibitor Complexes

compound 11	no. of crystals	no. of obsvns	no. of reflns	R_{merge}[c]	R_{frac}[d]
ATG[a]	2	75140	13028	0.097	0.15
ATDG[b]	1	36851	11741	0.118	0.20
b	2	50824	12206	0.096	0.14
c	2	49008	10752	0.068	0.19
d	2	50552	12388	0.070	0.19
k	1	18030	7212	0.085	0.18
l	1	19782	9391	0.127	0.26
m	3	75262	12377	0.119	0.18
h	1	30621	11393	0.128	0.17
i	1	32569	10523	0.093	0.19
j	1	18152	7661	0.069	0.19
f	1	20702	9851	0.120	0.16

[a] 8-Amino-9-(2-thienylmethyl)guanine. [b] 8-Amino-9-deaza-9-(3-thienylmethyl)guanine (data collected using a San Diego Multiwire System area detector). [c] R_{merge} is the R factor on intensities for merging symmetry-related reflections. [d] R_{frac} is the percent change between native and scaled PNP/inhibitor structure factor data.

Sutherland PS300 interactive computer graphics workstation using the computer graphics program FRODO. Idealized models were constructed for each inhibitor and then manually fitted to the difference electron density by varying torsion angles and overall orientation and position. The final coordinates were stored for further comparison and computational analysis.

Computer Modeling Studies. The initial model for the molecular modeling studies was derived from coordinates for PNP with guanosine and phosphate positioned in the active site. Coordinates for the protein atoms were based on the native X-ray structure that had been refined at 2.8-Å resolution. Coordinates for the purine ring and ribose were based on the structure of the 5'-deoxy-5'-iodoformycin B complex that was derived from X-ray electron density maps calculated at 3.2-Å resolution while coordinates for the phosphate group were derived from the sulfate ion that occupies the phosphate binding site in the crystal structure. Later, a second model was derived from the coordinates of the PNP/guanine complex that had been refined at 2.8-Å resolution. This model incorporated conformational changes in the protein atoms, particularly for residues 241 to 265, that were consistently observed for PNP/inhibitor complexes.

Construction of the computer models (initial and revised) used for the computational studies was accomplished as follows. Coordinates for the PNP monomer were obtained from X-ray diffraction studies in PDB[67] format and reformatted for the MacroModel/BATCHMIN program,[39] which was used for all molecular modeling studies involving molecular mechanics-based molecular energetics. Coordinates for the PNP trimer were then obtained by application of the C3 symmetry operation, and the sulfate ion was changed to phosphate. Two strategies for the total charge on phosphate were considered: (1) One in which dihydrogen phosphate is hydrogen bonded to His-86 via one of its hydroxyl groups; (2) One in which monohydrogen phosphate is hydrogen bonded to the protonated form of His-86. During the course of our molecular modeling studies, both approaches were employed without significant alteration of the results reported herein for 9-(arylmethyl)-9-deazaguanines in which dihydrogen phosphate was used.

Employing a strategy similar to the one previously described for exploring the conformational space available to inhibitors of thermolysin,[11] a shell of residues surrounding the binding site and lying within 7 Å of the purine (or purine nucleoside) and phosphate were included in the molecular energetics calculations. Thus, chains of complete residues were selected for molecular energetics calculations if any atom of the residue was within a 7 Å radius of either the inhibitor or phosphate moiety. The entire residue containing such an atom was selected for molecular energetics, and the chains of residues were produced so that the ends of the chains were extended out to the α-carbon atom of the adjacent residue. As a result of this operation, about 300 atoms were incorporated into the model. In addition, explicit hydrogen atoms were added to the phenyl groups of residues Phe-159 (from the B subunit) and residue Phe-200 (from the A subunit). His-

257A was tautomerized so that the N–H group was directed toward the solvent interface. Prior to conducting molecular modeling studies using this model, constrained energy minimization was performed using a parabolic restraining potential applied to all atoms of the model with a force constant of 500 kJ/Å[11] in order to refine it.

In order to determine the bound conformation of potential inhibitors in the PNP binding site, Monte Carlo/Energy Minimization (MC/EM) conformational searches[11,42] were performed. These inhibitors were docked to the PNP binding site by overlapping the purine ring of the inhibitor with the ligand contained in the model: initially guanosine and later guanine. After superimposing the inhibitor, the ligand used for alignment was removed and then the inhibitor was subjected to the MC/EM conformational search procedure. As previously described,[11] a distance-dependent dielectric constant of 2r was employed in these calculations. The low energy structures were evaluated qualitatively using molecular graphics analysis.[68] Initially, the force constants used for the parabolic restraining potentials were virtually identical to those described previously.[11] Later, force constants proportional to the crystallographically determined B-factors were employed and yielded slightly better agreement between computed structures relative to those determined crystallographically. In this procedure, which is somewhat different from the one described previously,[11] the following residues were subjected to the energy minimization part of the MC/EM procedure with weak parabolic anchoring potentials (force constant <2.0 kcal/Å²; proportional to the crystallographic B-factors): His-257, Phe-159 (B subunit), Phe-200, Met-219, Thr-242, Asn-243, Lys-244, Glu-201, Asn-256, Glu-258. In addition, the following other residues are also subjected to energy minimization with a parabolic anchoring constant of 25.0 kcal/Å²: Tyr-88, His-86, Arg-84, Gly-218, Val-195, Ser-199, Ser-33, Gly-118, Ala-116, Asn-115, Tyr-192, Thr-221, Thr-114, Ser-220, Val-217, Ala-117, Gly-32. These residues were selected based on the presence of at least one atom of the residue within 5 Å of the ligand and phosphate moieties. The phosphate ion was anchored with a parabolic anchoring force constant of 0.01 kcal/Å². Polar hydrogens within the binding site were not subjected to these restraints in order to allow proper hydrogen bonding geometries.

Initial molecular modeling studies were directed toward understanding how 9-(2-thienylmethyl)-8-aminoguanine (ATG)[37] docked within the binding site of PNP. Our assumption was that if molecular modeling studies were to be of value in prioritizing potential compounds for organic synthesis, it would be necessary to (at least) be able to estimate their binding geometry in the PNP active site. Subsequent analysis, of course, would be required to estimate the relative binding affinity of these compounds. Nonetheless, our first task was to attempt to compute the binding geometry of our lead compound in the PNP active site. Then, later comparison with the model derived from X-ray diffraction data would allow us first to determine the accuracy of our computational approach and then refine our methods as necessary. For this (and subsequent studies) it was assumed that the purine ring of the inhibitor would reside in a location within the PNP binding site that coincided with the position of the heterocyclic ring of either guanine or 5'-deoxy-5'-iodoformycin B (see above). Since all of the potential PNP inhibitors subjected to computer modeling studies were guanine analogs, the task of determining the binding geometry of these inhibitors was reduced to the problem of finding the bound conformation of the inhibitors. These studies yielded as the global minimum energy conformer a structure in which the thiophene ring was observed to lie within the hydrophobic pocket formed by Phe-159 (subunit B), Phe-200, His-257, and Met-219, as subsequently observed crystallographically. Table IV lists representative results for a number of 9-aryl-9-deazaguanines reported herein. In all cases, one of the low energy conformers obtained from the Monte Carlo/Energy Minimization procedure agreed favorably with the structure observed in the X-ray crystallographic studies.

References

(1) Erickson, J.; Neidhart, D. J.; VanDrie, J.; Kempf, D. J.; Wang, X. C.; Norbeck, D. W.; Plattner, J. J.; Rittenhouse, J. W.; Turon, M.; Wideburg, N.; Kohlbrenner, W. E.; Simmer, R.; Helfrich, R.; Paul, D. A.; Knigge, M. Design, Activity, and 2.8 Å Crystal Structure of a C$_2$ Symmetric Inhibitor Complexed to HIV-1 Protease. *Science* **1990**, *249*, 527–533.

(2) Appelt, K.; Bacquet, R. J.; Bartlett, C. A.; Booth, C. L. J.; Freer, S. T.; Fuhry, M. A. M.; Gehring, M. R.; Herrmann, S. M.; Howland, E. F.; Janson, C. A.; Jones, T. R.; Kan, C.-C.; Kathardekar, V.; Lewis, K. K.; Marzoni, G. P.; Matthews, D. A.; Mohr, C.; Moomaw, E. W.; Morse, C. A.; Oatley, S. J.; Ogden, R. C.; Reddy, M. R.; Reich, S. H.; Schoettlin, W. S.; Smith, W. W.; Varney, M. D.; Villafranca, J. E.; Ward, R. W.; Webber, S.; Webber, S. E.; Welsh, K. M.; White, J. Design of Enzyme Inhibitors Using Iterative Protein Crystallographic Analysis. *J. Med. Chem.* **1991**, *34*, 1925–1934.

(3) For a preliminary account of our work, see Ealick, S. E.; Babu, Y. S.; Bugg, C. E.; Erion, M. D.; Guida, W. C.; Montgomery, J. A.; Secrist, J. A., III. Application of Crystallographic and Modeling Methods in the Design of Purine Nucleoside Phosphorylase Inhibitors. *Proc. Natl. Acad. Sci. U.S.A.* **1991**, *88*, 11540–11544.

(4) McCammon, J. A.; Harvey, S. C. *Dynamics of Proteins and Nucleic Acids*; Cambridge Univ.: New York, 1987.

(5) Van Gunsteren, W. F.; Weiner, P. K., Eds. *Computer Simulation of Biomolecular Systems: Theoretical and Experimental Applications*; Escom Science: The Netherlands, 1989.

(6) DesJarlais, R. L.; Sheridan, R. P.; Dixon, J. S.; Kuntz, I. D.; Venkataraghavan, R. Docking Flexible Ligands to Macromolecular Receptors by Molecular Shape. *J. Med. Chem.* **1986**, *29*, 2149.

(7) Hart, T.; Read, R. J. A Multiple-Start Monte Carlo Docking Method. *Proteins* **1992**, *13*, 206–222.

(8) Caflisch, A.; Neiderer, P.; Anliker, M. Monte Carlo Docking of Oligopeptides to Proteins. *Proteins* **1992**, *13*, 223–230.

(9) Meng, E. C.; Shoichet, B. K.; Kuntz, I. D. Automated Docking with Grid-Based Energy Evaluation. *J. Comput. Chem.* **1992**, *13*, 505–524.

(10) Leach, A. R.; Kuntz, I. D. Conformational Analysis of Flexible Ligands in Macromolecular Receptor Sites. *J. Comput. Chem.* **1992**, *13*, 730–748.

(11) Guida, W. C.; Bohacek, R. S.; Erion, M. D. Probing the Conformational Space Available to Inhibitors in the Thermolysin Active Site Using Monte Carlo/Energy Minimization Techniques. *J. Comput. Chem.* **1992**, *13*, 214–228.

(12) Kim, B. K.; Cha, S.; Parks, R. E., Jr. Purine Nucleoside Phosphorylase from Human Erythrocytes. *J. Biol. Chem.* **1968**, *243*, 1763–1770.

(13) Zannis, V.; Doyle, D.; Martin, D. W., Jr. Purification and Characterization of Human Erythrocyte Purine Nucleoside Phosphorylase and Its Subunits. *J. Biol. Chem.* **1978**, *253*, 504–510.

(14) Ghangas, G.; Reem, G. H. Characterization of the Subunit Structure of Human Placental Nucleoside Phosphorylase by Immunochemistry. *J. Biol. Chem.* **1979**, *254*, 4233–4237.

(15) Wiginton, D. A.; Coleman, M. S.; Hutton, J. J. Characterization of Purine Nucleoside Phosphorylase from Human Granulocytes and Its Metabolism of Deoxyribonucleosides. *J. Biol. Chem.* **1980**, *255*, 6663–6669.

(16) Price, V. E.; Otey, M. C.; Plesner, P. Preparation of Nucleoside Phosphorylase from Calf Spleen. *Methods Enzymol.* **1955**, *2*, 448–453.

(17) Lewis, A. S.; Glantz, M. D. Bovine Brain Purine-Nucleoside Phosphorylase Purification, Characterization, and Catalytic Mechanism. *Biochemistry* **1976**, *15*, 4451–4457.

(18) Lewis, A. S.; Glantz, M. D. Monomeric Purine Nucleoside Phosphorylase from Rabbit Liver. *J. Biol. Chem.* **1976**, *251*, 407–413.

(19) Murakami, K.; Mitsui, A.; Tsushima, K. Purine Nucleoside Phosphorylase of Chicken Liver. *Biochim. Biophys. Acta* **1971**, *235*, 99–105.

(20) Murakami, K.; Tsushima, K. Crystallization and Some Properties of Purine Nucleoside Phosphorylase From Chicken Liver. *Biochim. Biophys. Acta* **1975**, *384*, 390–398.

(21) Jensen, K. F.; Nygaard, P. Purine Nucleoside Phosphorylase from *Escherichia coli* and *Salmonella typhimurium*. *Eur. J. Biochem.* **1975**, *51*, 253–265.

(22) Schimandle, C. M.; Tanigoshi, L.; Mole, L. A.; Sherman, I. W. Purine Nucleoside Phosphorylase of the Malarial Parasite, *Plasmodium lophurae*. *J. Biol. Chem.* **1985**, *260*, 4455–4460.

(23) Edwards, Y. H.; Edwards, P. A.; Hopkinson, D. A. A Trimeric Structure for Mammalian Purine Nucleoside Phosphorylase. *FEBS Lett.* **1973**, *32*, 235–237.

(24) Ikezawa, Z.; Nishino, T.; Murakami, K.; Tsushima, K. Purine Nucleoside Phosphorylase from Bovine Liver. *Comp. Biochem. Physiol. B: Comp. Biochem.* **1978**, *60B*, 111–116.

(25) Murakami, K.; Tsushima, K. Molecular Properties and a Nonidentical Trimeric Structure of Purine Nucleoside Phosphorylase From Chicken Liver. *Biochim. Biophys. Acta* **1976**, *453*, 205–210.

(26) Ward, R. D.; McAndrew, B. J.; Wallis, G. P. Purine Nucleoside Phosphorylase Variation in the Brook Lamprey, *Lampetra planeri* (Bloch) (Petromyzone, Agnatha): Evidence for a Trimeric Enzyme Structure. *Biochem. Genet.* **1979**, *17*, 251–256.

(27) Savage, B.; Spencer, N. Partial Purification and Properties of Purine Nucleoside Phosphorylase from Rabbit Erythrocytes. *Biochem. J.* **1977**, *167*, 703–710.

(28) Agarwal, R. P.; Parks, R. E., Jr. Purine Nucleoside Phosphorylase from Human Erythrocytes. *J. Biol. Chem.* **1969**, *244*, 644–647.

(29) Stoeckler, J. D.; Agarwal, R. P.; Agarwal, K. C.; Schmid, K.; Parks, R. E., Jr. Purine Nucleoside Phosphorylase from Human Erythrocytes: Physicochemical Properties of the Crystalline Enzyme. *Biochemistry* **1978**, *17*, 278–283.

(30) Lewis, A. S.; Lowy, B. A. Human Erythrocyte Purine Nucleoside Phosphorylase: Molecular Weight and Physical Properties. *J. Biol. Chem.* **1979**, *254*, 9927–9932.

(31) Williams, S. R.; Goddard, J. M.; Martin, D. W., Jr. Human Purine Nucleoside Phosphorylase cDNA Sequence and Genomic Clone Characterization. *Nucleic Acids Res.* **1984**, *12*, 5779–5787.

(32) Giblett, E. R.; Ammann, A. J.; Wara, D. W.; Sandman, R.; Diamond, L. K. Nucleoside-Phosphorylase Deficiency in a Child With Severely Defective T-Cell Immunity and Normal B-Cell Immunity. *Lancet* **1975**, *i*, 1010–1013.

(33) Stoop, J. W.; Zegers, B. J. M.; Hendricks, G. F. M.; Siegenbeek van Heukelom, L. H.; Staal, G. E. J.; de Bree, P. K.; Wadman, S. K.; Ballieux, R. E. Purine Nucleoside Phosphorylase Deficiency Associated With Selective Cellular Immunodeficiency. *N. Engl. J. Med.* **1977**, *296*, 651–655.

(34) Rich, K. C.; Arnold, W. J.; Palella, T.; Fox, I. H. Cellular Immune Deficiency With Autoimmune Hemolytic Anemia in Purine Nucleoside Phosphorylase Deficiency. *Am. J. Med.* **1979**, *67*, 172–176.

(35) Stoeckler, J. D.; Ealick, S. E.; Bugg, C. E.; Parks, R. E., Jr. Design of Purine Nucleoside Phosphorylase Inhibitors. *Fed. Proc.* **1986**, *45*, 2773–2778.

(36) Stoeckler, J. D. Purine Nucleoside Phosphorylase: A Target for Chemotherapy. In *Developments in Cancer Chemotherapy*; Glazer, R. I., Ed.; CRC Press: Boca Raton, 1984; pp 35–60.

(37) Sircar, J. C.; Gilbertsen, R. B. Purine Nucleoside Phosphorylase (PNP) Inhibitors: Potentially Selective Immunosuppressive Agents. *Drugs Future* **1988**, *13*, 653–668.

(38) Ealick, S. E.; Rule, S. A.; Carter, D. C.; Greenhough, T. J.; Babu, Y. S.; Cook, W. J.; Habash, J.; Helliwell, J. R.; Stoeckler, J. D.; Parks, R. E., Jr.; Chen, S.-f.; Bugg, C. E. Three-dimensional Structure of Human Erythrocytic Purine Nucleoside Phosphorylase at 3.2 Å Resolution. *J. Biol. Chem.* **1990**, *265*, 1812–1820.

(39) Mohamadi, F.; Richards, N. G. J.; Guida, W. C.; Liskamp, R.; Lipton, M.; Caufield, C.; Chang, G.; Hendrickson, T.; Still, W. C. Macro-Model - - An Integrated Software System for Modeling Organic and Bioorganic Molecules Using Molecular Mechanics. *J. Comput. Chem.* **1990**, *11*, 440–467.

(40) Weiner, S. J.; Kollman, P. A.; Case, D. A.; Singh, U. C.; Ghio, C.; Alagona, G.; Profeta, S., Jr.; Weiner, P. A New Force Field for Molecular Mechanical Simulation of Nucleic Acids and Proteins. *J. Am. Chem. Soc.* **1984**, *106*, 765–784.

(41) Weiner, S. J.; Kollman, P. A.; Nguyen, D. T.; Case, D. A. An All Atom Force Field for Simulations of Proteins and Nucleic Acids. *J. Comput. Chem.* **1986**, *7*, 230–252.

(42) Chang, G.; Guida, W. C.; Still, W. C. An Internal Coordinate Monte Carlo Method for Searching Conformational Space. *J. Am. Chem. Soc.* **1989**, *111*, 4379–4386.

(43) Tuttle, J. V.; Krenitsky, T. A. Effects of Acyclovir and Its Metabolites on Purine Nucleoside Phosphorylase. *J. Biol. Chem.* **1984**, *259*, 4065–4069.

(44) Stoeckler, J. D.; Cambor, C.; Kuhns, V.; Chu, S.-H.; Parks, R. E., Jr. Inhibitors of Purine Nucleoside Phosphorylase. *Biochem. Pharmacol.* **1982**, *31*, 163–171.

(45) Shewach, D. S.; Chern, J.-W.; Pillote, K. E.; Townsend, L. B.; Daddona, P. E. Potentiation of 2'-Deoxyguanosine Cytotoxicity by a Novel Inhibitor of Purine Nucleoside Phosphorylase, 8-Amino-9-benzylguanine. *Cancer Res.* **1986**, *46*, 519–523.

(46) Stoeckler, J. D.; Ryden, J. B.; Parks, R. E., Jr.; Chu, M.-Y.; Lim, M.-L.; Ren, W.-Y.; Klein, R. S. Inhibitors of Purine Nucleoside Phosphorylase: Effects of 9-Deazapurine Ribonucleosides and Synthesis of 5'-Deoxy-5'-iodo-9-deazainosine. *Cancer Res.* **1986**, *46*, 1774–1778.

(47) Halazy, S.; Ehrhard, A.; Danzin, C. 9-(Difluorophosphonoalkyl)-guanines as a New Class of Multisubstrate Analogue Inhibitors of Purine Nucleoside Phosphorylase. *J. Am. Chem. Soc.* **1991**, *113*, 315–317.

(48) Mamont, P. S.; Weibel, M.; Danzin, C.; Halazy, S. Effects of 9-(Difluorophosphonoalkyl)guanines, A New Class of Multisubstrate Analogue Inhibitors of Purine Nucleoside Phosphorylase in Cultured Human Leukemic Lymphoblast Molt-4 Cells. *Int. J. Purine Pyrimidine Res.* **1991**, *2* (Suppl. 1), 62.

(49) Lim, M. I.; Klein, R. S.; Fox, J. J. A New Synthesis of Pyrrolo[3,2-*d*]pyrimidines ("9-Deazapurines") Via 3-Amino-2-carboalkoxypyrroles. *J. Org. Chem.* **1979**, *44*, 3826–3829.

(50) Lim, M.-I.; Klein, R. S.; Fox, J. J. Synthesis of the Pyrrolo[3,2-*d*]pyrimidine C-Nucleoside Isostere of Inosine. *Tetrahedron Lett.* **1980**, *21*, 1013–1016.

(51) Lim, M.-I.; Ren, W.-Y.; Otter, B. A.; Klein, R. S. Synthesis of "9-Deazaguanosine" and Other New Pyrrolo[3,2-*d*]pyrimidine C-Nucleosides. *J. Org. Chem.* **1983**, *48*, 780–788.

(52) The systematic name for this ring system is 2-amino-4-oxo-3*H*,5*H*-pyrrolo[3,2-*d*]pyrimidine.

(53) Netherlands Patent 6,610,204, 1967; New Cyclic Thioimidates. *Chem. Abstr.* **1968**, *68*, 39631K.

(54) Profitt, J. A.; Watt, D. S.; Corey, E. J. A Reagent for the α,β Reduction of Conjugated Nitriles. *J. Org. Chem.* **1975**, *40*, 127–128.

(55) U.S. Patent 4,279,903, 1981.

(56) Skorcz, J. A.; Suh, J. T.; Judd, C. I.; Finkelstein, M.; Conway, A. C. Benzocyclobutene Derivatives. Oximes With Muscle Relaxant Characteristics. *J. Med. Chem.* **1966**, *9*, 656–659.

(57) Anderson, E. L.; Casey, J. E., Jr.; Greene, L. C.; Lafferty, J. J.; Reiff, H. E. Synthesis and Muscle Relaxant Properties of 3-Amino-4-arylpyrazoles. *J. Med. Chem.* **1964**, *7*, 259–268.

(58) Lim, M. I.; Klein, R. S. Synthesis of "9-Deazaadenosine", A New Cytotoxic C-Nucleoside Isostere of Adenosine. *Tetrahedron Lett.* **1981**, *22*, 25–28.

(59) For a review, see Taylor, E. C.; McKillop, A. Chemistry of Cyclic Enaminonitriles and O-Aminonitriles. *Adv. Org. Chem.* **1970**, *7*, 272.

(60) Yamazaki, A.; Okutsu, M. Cyclization of 5-Amino-1-β-D-ribofuranosylimidazole-4-carboxamide (AICA-riboside): A Review. *J. Heterocycl. Chem.* **1978**, *15*, 353–358.

(61) Lewis, A. F.; Townsend, L. B. Pyrazolopyrimidine Nucleosides. 13. Synthesis of the Novel C-Nucleoside 5-Amino-3-(β-D-ribofuranosyl)pyrazolo[4,3-*d*]pyrimidin-7-one, a Guanosine Analogue Related to the Nucleoside Antibiotic Formycin B. *J. Am. Chem. Soc.* **1982**, *104*, 1073–1077.

(62) Subject of another publication to be submitted.

(63) Burley, S. K.; Petsko, G. A. Aromatic-Aromatic Interaction: A Mechanism of Protein Structure Stabilization. *Science* **1985**, *229*, 23–28.

(64) Casari, G.; Sippl, M. J. Structure-derived Hydrophobic Potential. Hydrophobic Potential Derived from X-ray Structures of Globular Proteins is able to Identify Native Folds. *J. Mol. Biol.* **1992**, *224*, 725–732.

(65) Still, W. C.; Kahn, M.; Mitra, A. Rapid Chromatographic Technique for Preparative Separations With Moderate Resolution. *J. Org. Chem.* **1978**, *43*, 2923–2925.

(66) Stoeckler, J. D.; Parks, R. E., Jr. Purine Nucleoside Phosphorylase. *Methods Pharmacol.* **1985**, *6*, 147–162.

(67) Bernstein, F. C.; Koetzle, T. F.; Williams, G. J. B.; Meyer, E. F., Jr.; Brice, M. D.; Rodgers, J. R.; Kennard, O.; Shimanouchi, T.; Tasumi, M. The Protein Data Bank: A Computer-based Archival File for Macromolecular Structures. *J. Mol. Biol.* **1977**, *112*, 535–542.

(68) Bohacek, R. S.; McMartin, C. M. Definition and Display of Steric, Hydrophobic, and Hydrogen-Bonding Properties of Ligand Binding Sites in Proteins Using Lee and Richards Accessible Surface: Validation of a High-Resolution Graphical Tool for Drug Design. *J. Med. Chem.* **1992**, *35*, 1671–1684.